

University  
of Basel

**ETH** zürich

MASTER'S THESIS

---

# **Studying the Electrophysiological Phenotype of Human Dopaminergic Neurons with High-Density Microelectrode Arrays**

---

*Author:*

Gustavo PRACK

*Supervisors:*

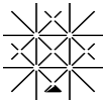
Dr. Manuel SCHRÖTER  
Prof. Henning STAHLBERG

*A thesis submitted in fulfillment of the requirements  
for the degree of Master of Science in Nanosciences*

*in the*

Bio Engineering Laboratory (BEL)  
Department of Biosystems Science and Engineering (D-BSSE)

Juli 26, 2019



**Erklärung zur wissenschaftlichen Redlichkeit**  
(beinhaltet Erklärung zu Plagiat und Betrug)

Masterarbeit

Titel der Arbeit (*Druckschrift*):

Studying the Electrophysiological Phenotype of  
Human Dopaminergic Neurons with High-Density  
Microelectrode Arrays

Name, Vorname (*Druckschrift*): Prack, Gustavo

Matrikelnummer: 13-051-750

Mit meiner Unterschrift erkläre ich, dass mir bei der Abfassung dieser Arbeit nur die darin angegebene Hilfe zuteil wurde und dass ich sie nur mit den in der Arbeit angegebenen Hilfsmitteln verfasst habe.

Ich habe sämtliche verwendeten Quellen erwähnt und gemäss anerkannten wissenschaftlichen Regeln zitiert.

Diese Erklärung wird ergänzt durch eine separat abgeschlossene Vereinbarung bezüglich der Veröffentlichung oder öffentlichen Zugänglichkeit dieser Arbeit.

☒ ja    ☐ nein

Ort, Datum: Basel, 26.07.2019

Unterschrift:

*Dieses Blatt ist in die Bachelor-, resp. Masterarbeit einzufügen.*

UNIVERSITY OF BASEL  
Philosophisch-Naturwissenschaftliche Fakultät

## *Abstract*

Bio Engineering Laboratory (BEL)  
Department of Biosystems Science and Engineering (D-BSSE)

Master of Science in Nanosciences

### **Studying the Electrophysiological Phenotype of Human Dopaminergic Neurons with High-Density Microelectrode Arrays**

by Gustavo PRACK

Studying the animal nervous system and particularly the human brain reveals an astonishing and most complex marvel of nature. Given its accomplishments – all aspects of human culture, for instance – there is good reason for wanting to understand how the brain and the rest of the nervous system work. The debilitating and costly effects of neurological and psychiatric diseases add a further sense of urgency to this quest. Parkinson’s disease is a progressive neurodegenerative disorder causing loss of motor function due to degeneration of dopaminergic neurons on approximately 1 % of the population above the age of 60. Why degeneration occurs remains unsolved and currently there is no cure. However, progress in stem cell biology provided new avenues to study neurological disorders in patient-derived tissue. Moreover, advances in microelectrode array technology allows examination of electrically active cells at high spatial and temporal resolution. Here, we apply high-density microelectrode arrays to examine the development of cellular- and network phenotypes of induced pluripotent stem cell (iPSC)- and embryonic stem cell (ESC) lines. We compare iPSC-derived dopaminergic neurons from a healthy subject, to an isogenic cell line carrying the early-onset A53T  $\alpha$ -synuclein point mutation. Moreover, we investigate the electrophysiological consequences of the GBA1 deletion on ESC-derived dopaminergic neurons. Both mutations are considered as major risk factors for Parkinson’s disease. Therefore, we create a pipeline to characterize development of neuronal features at single cell- and network level.

## *Acknowledgements*

Listing everyone who contributed to this work would probably double the length of this document. Hence, as a symbol of my concerns, I would like to show my gratitude to everyone with a short but sincere "Thank You" to all.

That being said, I would still like to exclusively thank some of you without whom my work would not have been possible. First of all, I give my special thanks to my supervisor Manuel Schröter, whose enthusiasm for solving endless puzzles of the nervous system persuaded me to dedicate my master's thesis to this mesmerizing subject. He made it possible for me to complete this project and taught me everything I needed to realize it. Thus, I was lucky to get such great support and I am happy to tell that what I have learned went way beyond the topic.

I express my appreciation to Zahra Ehsaei, Marius Kaciulis and Professor Verdon Taylor from the Department of Biomedicine for supplying me with their valuable cells in collaboration with this project. Furthermore, I give my special thanks to Michele Fiscella, Giulio Zorzi and the whole MaxWell Biosystems team for providing me the measurement setup and training me on it.

I would also like to convey my gratitude to Henning Stahlberg, who took the responsibility as referee and is taking his time to support my work.

Also, I am extremely thankful to Professor Andreas Hierlemann, for being warmly integrated into his research group, where I was able to meet many great new personalities. They guaranteed a wonderful time during my project work and motivated me to start a PhD after accomplishing my master's degree.

Last but not least, I am eternally grateful to my parents for the opportunity to study what I am passionate about, together with my sister and girlfriend for providing me with unfailing support and continuous encouragement at any given time. It certainly would not have been possible without them.



# Contents

<b>Abstract</b>	<b>ii</b>
<b>Acknowledgements</b>	<b>iii</b>
<b>1 Introduction</b>	<b>1</b>
1.1 Cellular Components of the Nervous System . . . . .	1
1.1.1 Electrogenesis of Membrane Excitability . . . . .	2
1.2 Microelectrode Array Technology in Neuroscience . . . . .	4
1.3 Using Stem Cells to Study Neurological Disorders . . . . .	6
1.3.1 Adult and Embryonic Stem Cell . . . . .	6
1.3.2 Induced Pluripotent Stem Cell . . . . .	7
1.4 State of Research, Motivation and Aim . . . . .	7
<b>2 Materials and Methods</b>	<b>9</b>
2.1 Cell Cultures . . . . .	9
2.1.1 Cell Plating . . . . .	10
2.2 High-Density Microelectrode Array . . . . .	12
2.2.1 HD-MEA Recordings . . . . .	13
2.2.2 Spike Sorting . . . . .	13
2.3 Data Analysis . . . . .	14
2.3.1 Single Cell Analysis . . . . .	15
2.3.2 Network Analysis . . . . .	15
2.3.3 Principal Component Analysis and Correlations . . . . .	15
2.3.4 Repeated Measures Analysis of Variance . . . . .	16
<b>3 Results</b>	<b>17</b>
3.1 iPSC-Derived Neurons . . . . .	17
3.1.1 Development of iPSC-Derived Neurons and Astrocytes . . . . .	17
3.1.2 Single Cell Features . . . . .	18
3.1.3 Network Features . . . . .	19
3.1.4 Significance of Single Cell- and Network Features . . . . .	21
3.2 ESC-Derived Neurons . . . . .	23
3.2.1 Cell Culturing Media Effect . . . . .	23
3.2.2 Impact of GBA1 <sup>-/-</sup> on Spontaneous Activity . . . . .	24
<b>4 Discussion</b>	<b>25</b>
4.1 Defining the Neuronal Phenotype . . . . .	25
4.2 Inhibitory- and Excitatory Effects of Culturing Media . . . . .	26
4.3 GBA1 Affecting Network Creation . . . . .	27
<b>5 Conclusion and Outlook</b>	<b>28</b>
<b>A Appendix</b>	<b>29</b>

**References****55**

# List of Abbreviations

<b><math>\alpha</math>-syn</b>	<b><math>\alpha</math>-Synuclein</b>
<b>A53T</b>	Point Mutation of the $\alpha$ -Synuclein Protein
<b>AP</b>	Action Potential
<b>BP</b>	BrainPhys <sup>TM</sup> Neuronal Medium
<b>BDNF</b>	Brain-Derived Neurotrophic Factor
<b>cAMP</b>	cyclic-Adenosine Monophosphate
<b>CMOS</b>	Complementary-Metal Oxide Semiconductor
<b>CNS</b>	Central Nervous System
<b>DA</b>	Dopaminergic
<b>DIV</b>	Day <i>In Vitro</i>
<b>D-PBS</b>	Dulbecco's Phosphate-Buffered Saline
<b>DT</b>	Disease Type
<b>ESC</b>	Embryonic Stem Cell
<b>FP</b>	Field Potential
<b>FCDI</b>	FUJIFILM Cellular Dynamics Incorporated
<b>GBA1<sup>-/-</sup></b>	GBA1 gene knockout
<b>GD</b>	Gaucher Disease
<b>GDNF</b>	Glia Cell-Derived Neurotrophic Factor
<b>HD-MEA</b>	High Density Microelectrode Array
<b>iPSC</b>	induced Pluripotent Stem Cell
<b>LFP</b>	Local Field Potential
<b>MEA</b>	Microelectrode Array
<b>mFPP</b>	midbrain Floor Plate Progenitor
<b>NB</b>	Neurobasal <sup>TM</sup> Medium
<b>PCA</b>	Principal Component Analysis
<b>PD</b>	Parkinson's Disease
<b>PLO</b>	Poly-L-Ornithine
<b>PNS</b>	Peripheral Nervous System
<b>SNCA</b>	$\alpha$ -Synuclein Gene
<b>TGF<math>\beta</math>3</b>	Transforming Growth Factor $\beta$ -3
<b>WT</b>	Wild Type

# 1

## Introduction

The exploration of molecular, cellular, systemic, behavioral, and cognitive features in neuroscience, has revealed a stupendous biological machinery. Studying the nervous system of humans and other animals, and in particular the cells and connectivity of the human brain, has involved interdisciplinary collaborations between scientists from various fields. Even though some of the cellular components of neurons are similar to those of other organs, their quantity in the nervous system is remarkable. It is estimated that the human brain contains  $10^{11}$  neurons and perhaps three times as many glial cells. Furthermore, the number of distinct cell types in the nervous system is greater than in any other organ system which makes it possible to create such complicated networks and sophisticated behaviours [1, 2, 3].

In the past years, progress has been achieved in immunohistochemistry, single cell genetics, imaging and computational analysis. This facilitated identification of different neuronal subtypes, description of their molecular constituents, interpretation of neural coding, and characterization of functionalities in specific brain regions. Yet, many key questions regarding communication within the nervous system remain unsolved since the brain is a complex system and its activity runs in multiple temporal and spatial scales, requiring a wide-ranging set of technologies to address these scales. Therefore, innovations in experimental methods to observe, measure and analyze recorded brain activity are needed to understand the brain's complexity and increase our knowledge of its functions.

In this introductory chapter, the functions of the cellular components located in the nervous system will be briefly described and characterized in Sec. 1.1. Besides, Sec. 1.2 will outline the utility of microelectrode array technologies for the measurements of electrical signals of nerve cells. Moreover, progress in stem cell research in the past years will be introduced in Sec. 1.3, while demonstrating the advantages of embryonic stem cells and induced pluripotent stem cells for studies in neuroscience.

### 1.1 Cellular Components of the Nervous System

Histological studies of the Spanish neuroanatomist Santiago Ramón y Cajal and several successors led to the conclusion that the nervous system can be divided into two categories [4, 5]. The nerve cells, or neurons, and glial cells or simply glia.

Neurons generate various types of electrochemical signals, which are the key elements for transmitting and storing information in the brain. A schematic of a neuron is depicted in Fig. 1.1. Perhaps the most obvious morphological characteristics of neurons is their extensive arborization- i.e. their axonal projection and dendrites, which both arise from the neural cell body, or soma, that contains the cell nucleus. Dendritic

branches are the primary targets for synaptic inputs from the axon terminals of other neurons.

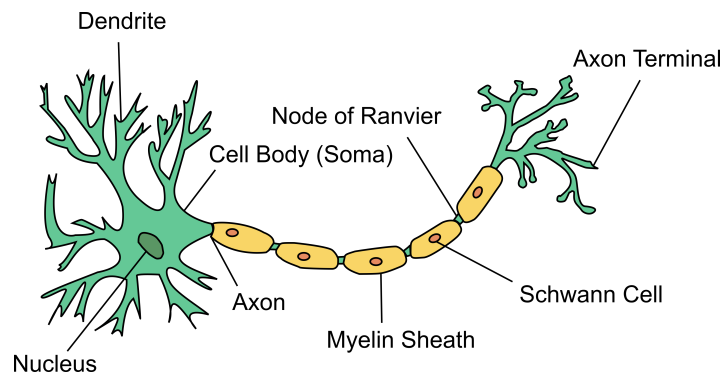


**Figure 1.1:** Cell morphology of a neuron. Axon with axon terminals and dendrites arise from the soma which houses the nucleus. During the myelination of the axon through Schwann cells in the PNS, gaps between the myelin sheaths arise, which are called nodes of Ranvier.

In contrast, glia support neuronal functions such as electrical signals rather than generating them [6, 7]. Moreover, glia play a central role in the development of the adult brain [8]. As essential contributors to the repair of a damaged nervous system, they act as stem cells [9]. In brain regions where regeneration is necessary, glia promote the regrowth of damaged neurons while preventing regeneration in regions where uncontrolled regrowth should be avoided [10].

In the mature nervous system, glial cells differentiate into three types, namely astrocytes, oligodendrocytes, and microglia cells. A major function of astrocytes, which can only be found in the central nervous system (CNS), is maintaining homeostasis at the synapse to regulating neuronal signaling [11]. Oligodendrocytes form a laminated, lipid-rich sheath called myelin around axons, which has important effects on the transmission speed of electrical signals. Since oligodendrocytes are also restricted to the CNS, in the peripheral nervous system (PNS), the myelinating cells are called Schwann cells, shown in Fig. 1.1. The uninsulated gaps between the myelin sheath, also known as nodes of Ranvier, contain various ion channels, which, *in vivo*, play a significant role in the regeneration of electrical signals. Finally, microglia are often considered as macrophages in the CNS. They are primarily phagocytes removing left-over of death cells from sites of injury or normal cell turnover. For the aim of this study we particularly focus on the electrophysiological property of a neuron.

### 1.1.1 Electrogenesis of Membrane Excitability

Neurons are the origin of electrical signaling in the nervous system. Although neurons are not intrinsically good conductors, they possess mechanisms that allow them to create electrical signals based on the flow of ions across their plasma membranes [12, 13]. The differences in concentrations of specific ions across nerve cell membranes generate electrical membrane potentials. Further, the membranes are selectively permeable to some of these ions. In turn, the ion concentrations and permeabilities are regulated by cell membrane proteins, as depicted in Fig. 1.2.

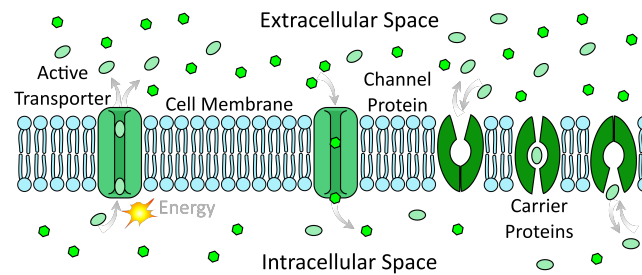


**Figure 1.2:** Active transporters, ion channels and carriers are responsible for ionic movements across the membranes. Transporters create ion concentration differences by actively transporting ions against their chemical gradients. Channels take advantage of these concentration gradients, allowing selected ions to diffuse down their chemical gradients. Carrier proteins transport molecules either passively through diffusion, or via secondary active transport.

The ion concentration gradients are mostly established by proteins known as active transporters, which actively move ions into or out of cells against their concentration gradients [14]. The selective permeability of membranes is due to ion channels. These are proteins that allow only certain kinds of ions to cross the membrane in the direction of their concentration gradients [15]. Thus, channels and transporters work against each other, and in so doing they can change the membrane potential. Carrier proteins can transport ions and molecules either passively through facilitated diffusion, or via secondary active transport.

One approach to study these electrical signals is to use an intracellular microelectrode to measure the potential difference between the inside and the outside of the cell. A typical microelectrode is a glass capillary, which is pulled to a very thin end and filled with a good electrical conductor, such as a metal wire or a concentrated salt solution. As soon as the microelectrode is inserted through the membrane of a neuron a negative potential can be recorded, indicating constant voltage in the membrane of an inactive neuron. This voltage, depicted as the dashed grey line in Fig. 1.3a, is called the resting membrane potential. Depending on the type of neuron this value is typically between -40 mV and -90 mV [16].

Electrical signals of neurons are caused by spontaneous activities to improve development of the neural network, or due to responses to different stimuli, which change the resting potential [17]. One example is the receptor potential, which is due to transient activation of sensory neurons by an external stimulus, such as light, sound, or heat [18]. These changes in potential are the first step in e.g. generating the sensation of vibrations of the skin in the somatic sensory system. Another type of electrical signal is associated with the communication between neurons at synaptic contacts. Activation of these synapses generate synaptic potentials, which allow the transmission of information from one neuron to another [19]. Finally, neurons also generate a special type of electrical signal that travels along their axons. This signal is called the action potential (AP) [13, 16]. The intra- and extracellular waveforms of an AP are shown in Fig. 1.3. Depending on whether the AP is measured with an intracellular- or an extracellular electrode, the signals obtained will look different. Intracellular electrodes measure the changing membrane potential generated by ion fluxes of approximately  $\Delta 100$  mV. In contrast, an extracellular electrode picks up the field potential (FP) generated by an AP of a neuron [20]. Hence, the amplitude is inverse due to the opposite charge distribution on the membrane outside. Moreover, the recorded FP amplitudes are significantly smaller ranging approximately between  $\Delta 10$   $\mu$ V and  $\Delta 1$  mV.

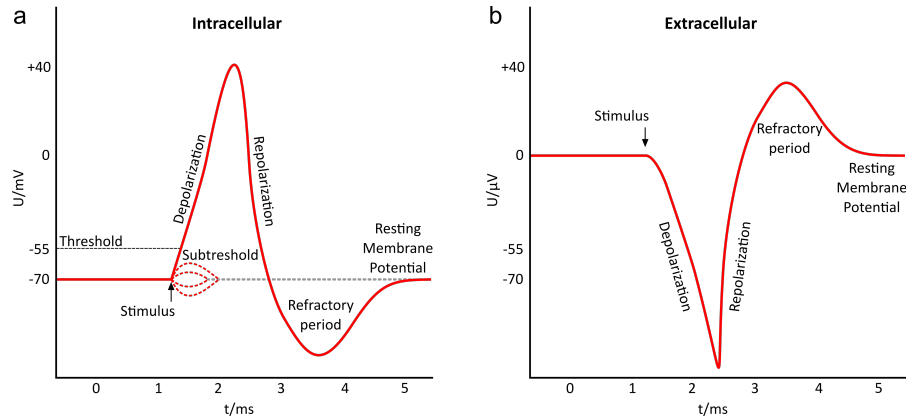


**Figure 1.3:** Schematics of an electrophysiological recording of an intracellular AP (a) and an extracellular AP (b) as a function of time, containing the different phases as the wave elongates through the axon of a neuron.

APs are responsible for transmission of information within the nervous system to its target organs. One way to induce an AP is the application of an electrical current across the membrane. If the current lowers the membrane potential (hyperpolarization), no AP is generated [21]. The same applies, if the delivered current increases the membrane potential, without exceeding a certain level called the threshold potential [22]. These subthreshold responses of the membrane potential are referred to as passive electrical responses. However, if a current is delivered in a way that the membrane potential of the nerve cell becomes more positive than the threshold potential (depolarization), an AP occurs.

## 1.2 Microelectrode Array Technology in Neuroscience

A central aim of modern neuroscience is to understand the connectivity of neuronal circuits and their physiological function. For this endeavour, electrophysiology has been the method of choice due to its ability to capture a variety of neural phenomena, ranging from the spiking activity of individual neurons to network dynamics among populations of neurons [23, 24, 25]. Patch-clamp, as an example, can be used to measure currents flows through single ion channels in the cell membrane. The function of single neurons is often investigated by directly measuring the intracellular voltage, using patch-clamp or a sharp microelectrode. Although intracellular recordings are very useful, their usage is often limited to only a few neurons per experiment [26]. On the other hand, metal electrodes, integrated into large arrays, so-called microelectrode arrays (MEAs), allow extracellular recordings via indirect measurements of larger cell populations. MEAs enable long-term recordings of both local field potentials (LFPs) and extracellular APs from a population of neurons at millisecond temporal resolution. Some MEAs also allow the perturbation of neuronal activity using electrical stimulation [27]. Therefore, MEAs have become an essential tool in basic and applied research, enabling to progress from the observation of the electrical behavior of single neurons toward the analysis of neural cell populations [28].

Fig. 1.4a illustrates the point-contact model of a neuron laying on the top of a substrate integrated electrode in a MEA with its analogous electrical circuit [29]. Such a model indicates that a tight seal between the neuron and electrode is needed to measure extracellular APs from isolated neurons. The cell membrane is represented

with an equivalent model based on the Hodgkin-Huxley model of the squid axon [30].  $C_M$  represents the capacitance across the neuronal membrane. The voltage-gated ion channels ( $K$  for potassium and  $N_a$  for sodium) are represented by non-linear conductance,  $g_K$  and  $g_{N_a}$ , and the leak is shown as a linear conductance,  $g_L$ . The reversal potentials that drive the flow of ions are represented by  $E_K$ ,  $E_{N_a}$ , and  $E_L$ . The ion flow is shown by  $I_K$ ,  $I_{N_a}$ ,  $I_L$ , and  $I_C$ . The other elements are described in the text.  $V_{rec}$  is the recorded voltage signal. Typical intracellular AP and extracellular AP recordings are shown. The location of the scissors indicates where the “cut” can be made to separate the neuron-electrode interface into two parts. For MEAs with a large number of densely arranged electrodes, so called high-density microelectrode arrays (HD-MEAs), it has been observed that signs of extracellular APs are also detected by electrodes relatively distant from the neuronal source [31]. This model, generalized in Fig. 1.4b, assumes that the MEA surface can be treated as an insulator separating the neuron-electrode interface into two parts: fluid-side and metal side [32]. This is valid, if the impedance on the metal-side seen by the electrodes is much larger than the fluid impedance of all frequencies.

For the fluid side, it is assumed that the MEA surface is an insulating infinite plane and the fluid a homogeneous isotropic medium [33, 34, 35]. Thus, the potential  $V_e$  at any given electrode  $e$  can be given solved using the following equation:

$$V_e = \frac{1}{2\pi\sigma} \sum \frac{I_n}{r_r}. \quad (1.1)$$

$I_n$  represents the  $n^{th}$  point current source and  $r_n$  the distance between point source and recording electrode, with  $n = 1, \dots, N$  and  $N$  the number of individual point sources. The distribution and decay of the signal over the MEA surface plane is highly correlated with the distance of the signal source from the surface, making it possible to estimate the distance between source and electrode.

For the metal-side, the input to the circuit is a low voltage source with the value corresponding to the potential resulting from the currents in the fluid. This voltage  $V_e$  is connected to the effective electrode impedance  $Z'_e$  which consists of  $R_{spread}$ ,  $R_m$ ,  $R_e$  and  $C_e$ . Here,  $R_{spread}$  represents the current that spreads from the electrode into the electrolyte.  $R_e$  and  $C_e$  are the double layer resistance and capacitance respectively, formed at the electrode-electrolyte interface.  $R_m$  is an additional resistance representing the metallic part of the microelectrode. The effective amplifier input impedance,  $Z'_a$ , is connected in series to  $Z'_e$ , which includes the actual input impedance of the amplifier  $Z_a$  and the shunting paths to ground outside the amplifier ( $R_s$  and  $C_s$ ) [33, 34].



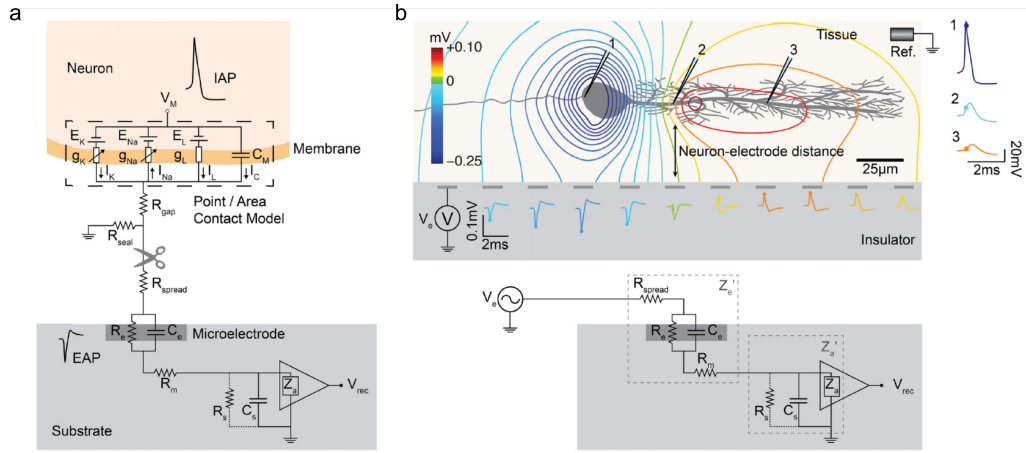


**Figure 1.4:** Schematics of a MEA neuron-electrode interface. (a) The classic point-contact model derived from Weis and Formherz [29]. (b) Generalized neuron-electrode interface separating the problem into upper-fluid-side and lower-metal-side. This model is derived from [33, 34, 35]. Figure is taken from Obien *et al.* [32].

Electrophysiological recording and stimulation with HD-MEAs *In Vitro*, have been used in a wide variety of neuroscience applications. Studies have recorded light-induced retinal ganglion cell activity using HD-MEAs, and action potential in cortical neurons [36, 31]. Additionally, data from acute slices of the cerebellum, cortex and culture cardiomyocytes have been studied [37, 38, 39]. Also, there are now studies that probed spontaneous and evoked electrical network activity of human induced pluripotent stem cell (iPSC)-derived neurons grown on conventional- and HD-MEAs [40, 41].

### 1.3 Using Stem Cells to Study Neurological Disorders

Stem cells have become a promising research field with the potential to study and effectively address some of the most severe neurological disorders. Stem cells are cells with the ability to generate identical cells for a lifetime through self-renewal and to generate mature cells of a particular tissue through differentiation. They can be categorized into three main types of stem cells: Adult stem cells, embryonic stem cells and induced pluripotent stem cells.

#### 1.3.1 Adult and Embryonic Stem Cell

Adult stem cells are a rare population of cells, located in differentiated tissues such as skeletal muscle, liver, bone marrow and brain [42]. They remain undifferentiated in the tissue, but continuously self-renew [43]. Adult stem cells differentiate into a limited number of mature cell types of the tissue of origin and are thus referred to as multipotent. An important function is the replacement of cells that are lost due to tissue turnover or injury, thus ensuring the maintenance of tissue homeostasis [44].

In contrast, embryonic stem cells (ESCs) are found in the blastocyst-stage of an early embryo. ESCs have the ability to form any fully differentiated cell of the body, hence denoted as pluripotent [45]. Pluripotent ESCs can be removed from the blastocyst and maintained in their undifferentiated stage(s) in cell culture.

### 1.3.2 Induced Pluripotent Stem Cell

In 2006, a major technological breakthrough in science and medicine was made. Using only four transcription factors, Takahashi and Yamanaka were able to generate cells from mouse fibroblasts with a gene expression profile and developmental potential similar to ESCs [46]. These cells are referred to as induced pluripotent stem cells (iPSCs). Just one year later, two research groups independently reported the generation of iPSCs from human fibroblasts [47, 48].

Evolving rapidly since 2007, human iPSC technology was a game changer for the fields of stem cell biology and regenerative medicine, as well as the fields of disease modelling and drug discovery. Compared with traditional cellular screens, the interest in phenotypic screening and the advantages of human iPSCs disease modelling *in vitro* are becoming increasingly popular. It offers many advantages, such as their human origin, easy accessibility, ability to differentiate into almost any cell type, expandability, prevention of ethical confrontations related to human ESCs and the capability to develop personalized medicine using patient-specific iPSCs. Consequently, iPSCs can provide large quantities of disease-relevant cells that were previously difficult to access, such as neurons. Since iPSCs, develop genetic variations among cell lines, data interpretation of disease-relevant phenotypes may still be complicated. However, modern genome editing technologies enable the introduction of specific mutations into iPSCs in order to evolve isogenic cell lines. [49, 50, 51]. Having similar genotypes, isogenic iPSC controls are essential when modeling sporadic diseases, in which phenotypic differences are expected to be small [52].

## 1.4 State of Research, Motivation and Aim

In this study, we will focus on cell lines carrying mutations considered as major risk factors in Parkinson's disease (PD). PD is a progressive neurodegenerative disorder affecting more than 1 % of the population over 60 [53, 54]. Nevertheless, a severe disease type referred to as young-onset PD also exist in patients at an earlier age. Their average life expectancy after diagnosis is 7 to 14 years [53, 54]. Common symptoms in PD patients are tremor, shaking, rigidity and slowness at initiating a movement [53, 54]. Moreover, 1/3 of the patients suffer from non-motor symptoms including loss of olfaction, depression and anxiety [55]. However, the causes of PD, and whether these symptoms are directly linked to the disease remains unclear [56]. Though, motor disorders are closely linked to damage and degeneration of dopaminergic (DA) neurons of the nigrostriatal pathway [53, 54]. The loss of DA neurons in the brain could also explain the loss of the olfactory sense, depression and anxiety. Affected DA neurons develop protein aggregates of misfolded  $\alpha$ -synuclein ( $\alpha$ -syn) called Lewy bodies. Thus, mutations in the alpha-synuclein gene (SNCA) are thought to play a major role in the development of PD [57, 58]. Still, why particularly DA neurons are affected is still not known and currently, there is no cure for PD.

In this MSc thesis project, we will probe human iPSC / ESC derived DA neurons using HD-MEAs and study their development *in vitro*. We will demonstrate that HD-MEA experiments are also useful to investigate the development of potential phenotypic differences between human wild type and two mutant disease DA neuron cell lines.

In the first study, we compare the development of DA neuronal cultures, at the cellular and network level and compare these features between a healthy WT iPSC-line, to an isogenic cell line carrying the A53T  $\alpha$ -syn mutation. Therefore, we simultaneously recorded cellular activity from 1'024 electrodes using state-of-the-art HD-MEA

technology and analyzed the data to conclude which features were most informative to predict the phenotype [59].

For the second study, we demonstrated how a culturing medium affects spontaneous cell activity which in turn influence the recording quality. Thus, we investigated the inhibiting and activating effect of two different culturing media on network activity of human derived ESC-lines with HD-MEA recording.

Furthermore, in a third study, we examined the electrophysiological impact of the GBA1 gene knockout throughout cell development on-chip. We thereby verified that the lack of this gene hinders proper creation of neuronal networks within a culture.

# 2

## Materials and Methods

In this section, we describe the methodology applied throughout all experimental procedures of this study. First, we introduce the human stem cell derived neuronal cultures used in this study (Sec. 2.1). Next, we outline the HD-MEA plating protocol and describe the required medium to culture them. In the following section, Sec. 2.2 we will present the experimental set up with its corresponding hard- and software. In order to study the development of neuronal cultures and potential phenotypic differences between the wild type and the mutant cell line, we analyzed neuronal activity at the single cell- and network-level. We therefore describe the pre-processed the HD-MEA data (spike sorting) and explain, which quantitative metrics were used to characterize neuronal cultures (Sec. 2.3).

### 2.1 Cell Cultures

Four different cell lines derived from two different cell types were investigated in three different experimental series. In the first experimental series, we tested two commercially available cell lines of iPSC-derived human midbrain floorplate DA neurons, co-cultured with human iPSC-derived astrocytes in order to improve cell development. The cells were differentiated in protocols licensed and adapted from the Lorenz Studer lab (Sloan Kettering Institute, New York City) and industrialized for scale at FUJIFILM Cellular Dynamics, Inc. (FCDI) [60]. Fully differentiated wild type (WT) iCell<sup>®</sup> DopaNeurons (>80 % pure midbrain DA neurons) with expression of relevant midbrain DA neuron markers were used as a control, exhibiting the relevant biology and functionalities [61]. The disease type (DT) examined in the same series were MyCell<sup>®</sup> DopaNeurons [62]. MyCell<sup>®</sup> DopaNeurons harbour the early onset mutation A53T in the SNCA gene which is one of the most highly penetrant and widely studied mutations linked to PD [63]. The A53T mutation renders  $\alpha$ -syn more susceptible to aggregation and accumulation, which are hallmark indicators of PD pathology [63]. As a support for the neural tissue, iCell<sup>®</sup> Astrocytes were added to both cell lines [64].

For the second and third experimental series, two cell lines of genetically engineered human ESC-derived neurons were provided by the lab of Professor Verdon Taylor (Fedele *et al.* in preparation, Department of Biomedicine, University of Basel). The WT was used as a control, however for the DT the GBA1 gene has been deleted (GBA1<sup>-/-</sup>). The GBA1 gene encodes the lysosomal enzyme GCase which mediates the hydrolysis of glucosylceramide and glucosylsphingosine to glucose and ceramide or sphingosine, respectively. GBA1 mutations cause the lysosomal storage disorder Gaucher disease (GD), and genome-wide association studies identified small nucleotide polymorphisms in GBA1 as one of the strongest genetic risk factors for PD [65]. To generate fully differentiated neurons, DA neuron progenitors were expanded *in vitro* following a standard midbrain floor plate progenitor (mFPP) protocol with some modifications as, illustrated

in Fig. 2.1 [66, 67]. After 20 days of expansion, the differentiating mFPP cells were finally passaged in order to be plated on HD-MEA chips. The day on which the cells were finally plated on the chip was referred to as day *in vitro* (DIV) 0.

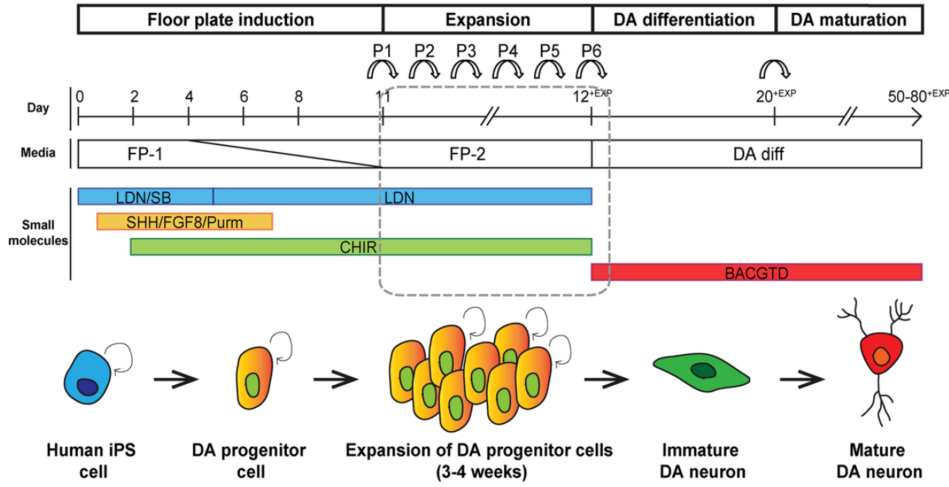


**Figure 2.1:** Schematic diagram for efficient expansion of in vitro DA neuron progenitors and final DA neuron maturation from human iPSCs. (a) In vitro DA neurons were generated using a standard mFPP protocol with some modifications [66]. After 11 days of neuralization and floor plate induction by adding signaling molecules such as SHH, FGF8 and CHIR-99021, mFPPs were amplified by cell passaging and maintained in culture for 3 - 4 weeks (6 passages in total as indicated by the arrows P1 - P6). Image taken from Fedeles *et al.* [67].

### 2.1.1 Cell Plating

To compare the electrical signaling across iPSC cultures and to study the development of different cell lines, cells had to be plated on the HD-MEA surfaces. Below, we provide the numbers and plating densities per chip in Tab. 2.1. For the first and third experimental series, WT and DT of iPSC-derived human midbrain floorplate DA neurons with astrocytes and genetically engineered human ESC-derived neurons were plated following a protocol approved by the Basel Stadt veterinary office according to Swiss federal laws.

**Sterilization:** As a first step, one day before the plating, all MEA chips and lids, to cover and protect HD-MEA surfaces, were sterilized to prevent cell contamination. Therefore, both the chips and lids were placed in petri dishes filled with 70% ethanol for 30 minutes. Next, the ethanol was removed and chips were rinsed three times with autoclaved ultrapure H<sub>2</sub>O. After aspirating all H<sub>2</sub>O from the chips and the lids, a Poly-L-ornithine (PLO) (Sigma, catalog number: P4957) coating was carried out to enable cell attachment on the electrode surface. All steps were carried out in a sterile environment, i.e. under a laminar flow hood.

**Coating:** 50  $\mu$ l of 100  $\mu$ g/ml PLO solution was added to the center of every chip, directly covering the electrodes and then incubated at 37°C for two hours. Next, the PLO solution was aspirated from the electrode surface and rinsed twice with 1 ml of sterile Dulbecco's Phosphate-Buffered Saline (D-PBS), without letting the surface drying out. After a final wash, every electrode surface was rinsed with 1 ml of ultrapure

H<sub>2</sub>O and aspirated afterwards. HD-MEA chips and the lids were then air-dried in a laminar flow hood overnight.

**Medium Preparation:** The cell culturing medium was based on BrainPhys™ Neuronal Medium (BP) and prepared as following: 47.5 ml of BP (Stem Cell Technologies, catalog number: 05790) was mixed with 1ml iCell Neural Supplement B (Cellular Dynamics International, M1029), 500  $\mu$ l iCell Nervous Supplement (Cellular Dynamics International, M1031), 500  $\mu$ l N-2 Supplement (ThermoFisher Scientific, catalog number: 17502048), 50  $\mu$ l laminin (Sigma, catalog number: L2020), and 500  $\mu$ l penicillin-Streptomycin (ThermoFisher Scientific, catalog number: 15140122).

80  $\mu$ l of 1 mg/mL stock laminin solution was mixed with prepared BP containing 1  $\mu$ g/ml laminin to obtain medium containing 80  $\mu$ g/ml laminin.

**Cell Plating:** For the plating, we pipetted 8  $\mu$ l of BP containing 80  $\mu$ g/ml laminin directly on the rectangular recording electrode area of every chip and left the chips in the incubator for 30 minutes at 37°C. Meanwhile, BP containing 1  $\mu$ g/ml laminin was equilibrated at room temperature and the neurons and astrocytes (1 ml cryovials) were immersed in a 37°C water bath for exactly three minutes. Next, neurons and astrocytes were transferred into sterile 50 ml centrifuge tubes and rinsed with 1 ml BP containing 1  $\mu$ g/ml (at room temperature) to recover any residual cells from the vial. Another 3 ml of BP containing 1  $\mu$ g/ml were added to the centrifuge tubes, yielding a total volume of 5 ml cells + medium. The tubes with cells were then centrifuged for 5 minutes at 380 x g ( $1.6 \cdot 10^3$  RPM). After centrifuging, the supernatant was removed and BP containing 80  $\mu$ g/ml laminin added to achieve a neuron to astrocytes concentration of  $10^4$  cells/ $\mu$ l and  $2 \cdot 10^3$  cells/ $\mu$ l respectively. Finally, the cell solution was transferred to a new 1.5 ml centrifuge tube and 10  $\mu$ l of this solution were added to the 8  $\mu$ l droplet of BP containing 80  $\mu$ g/ml laminin on each HD-MEA chip. All plated chips, containing  $10^5$  cells were then incubated at 37°C, 5 % CO<sub>2</sub> and 95 % humidity for 1 hour, covering each chip with a lid. After incubation the chips containing the cell droplets were filled up with 0.6 ml or 1.2 ml of BP depending on the ring size of the chips. 50 % of BP containing 1  $\mu$ g/ml medium was exchanged on the day after the plating; thereafter we exchanged 33 % medium twice a week.

The cell plating for the third experimental series was based on the same protocol. However, a density of  $50 \cdot 10^4$  cells were plated on every chip. The HD-MEAs for the second experiment, containing  $6 \cdot 10^3$  or  $3 \cdot 10^4$  cells per chip, were plated in the lab of Professor Verdon Taylor [67]. Their cell culturing medium was based on Neurobasal™ Medium (NB) and contained 24 ml NB (ThermoFisher Scientific, catalog number: 21103049), 250  $\mu$ l penicillin-Streptomycin (ThermoFisher Scientific, catalog number: 15070063), 250  $\mu$ l GlutaMax™ Supplement (ThermoFisher Scientific, 35050061) and 500  $\mu$ l B-27™ Supplement (ThermoFisher Scientific, catalog number: 17504044). Additionally, growth factors were added the medium to improve differentiation of not yet fully differentiated progenitors. These were 25  $\mu$ l brain-derived neurotrophic factor (BDNF), 19.8  $\mu$ l AA, 5  $\mu$ l glial cell-derived neurotrophic factor (GDNF), 2.5  $\mu$ l cyclic adenosine monophosphate (cAMP), 2.5  $\mu$ l DAPT and 2.5  $\mu$ l transforming growth factor beta-3 (TGF $\beta$ 3). Regular 50 % of the medium was changed every second day.

Cell Culture	# Neurons	# Astrocytes	# Chips
iCell <sup>®</sup> DopaNeurons + iCell <sup>®</sup> Astrocytes	$8 \cdot 10^4$	$2 \cdot 10^4$	10
MyCell <sup>®</sup> DopaNeurons + iCell <sup>®</sup> Astrocytes	$8 \cdot 10^4$	$2 \cdot 10^4$	10
ESC-derived neurons (WT)	$6 \cdot 10^3$	-	6
ESC-derived neurons (WT)	$3 \cdot 10^4$	-	6
ESC-derived neurons (DT)	$6 \cdot 10^3$	-	6
ESC-derived neurons (DT)	$3 \cdot 10^4$	-	6
ESC-derived neurons (WT)	$5 \cdot 10^4$	-	10
ESC-derived neurons (DT)	$5 \cdot 10^4$	-	10

**Table 2.1:** Densities of cell cultures plated per chip. First experimental series (top) shows densities and chip numbers of iCell<sup>®</sup> DopaNeurons with iCell<sup>®</sup> Astrocytes for WT cultures and MyCell<sup>®</sup> DopaNeurons + iCell<sup>®</sup> Astrocytes for DT (A53T). Second (middle) and third (bottom) experimental series show densities and chip numbers of genetically engineered human ESC-derived neurons for WT and DT (GBA1<sup>-/-</sup>).

## 2.2 High-Density Microelectrode Array

All recordings were performed on a complementary-metal-oxide-semiconductor (CMOS)-based high-density MEA device (see Fig. 2.2, [68, 59]). It was developed in the Bio Engineering Laboratory (BEL, D-BSSE ETH Zürich) and commercialized by MaxWell Biosystems AG, a spin-off company of the BEL [59, 68]. The HD-MEA of this study features an active sensing area of  $3.85 \times 2.10 \text{ mm}^2$  with 26'400 platinum microelectrodes. The electrodes are arranged in a grid-like configuration with a center-to-center pitch of  $17.5 \mu\text{m}$ , yielding an electrode density of 3'265 microelectrodes per  $\text{mm}^2$ . A subset of 1'024 electrodes connected to the corresponding readout channels can simultaneously be measured at a sampling rate of 20 kHz and a readout noise in the AP signal band (300 Hz - 10 kHz) of  $2.4 \mu\text{V}_{\text{rms}}$  [69].

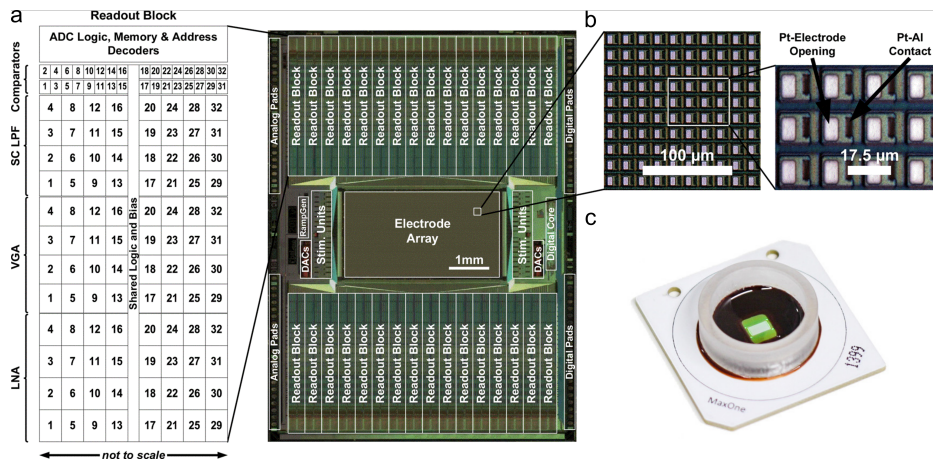


**Figure 2.2:** CMOS HD-MEA system architecture. (a) Micrograph of the CMOS device. The 1'024 readout channels are at the top and bottom of the  $3.85 \times 2.1 \text{ mm}^2$  electrode array. (b) Zoom of the electrode sensing area. (c) MaxWell Biosystems' MaxOne Single-Well HD-MEA [68]. Figure adapted from Ballini *et al.* [69].



### 2.2.1 HD-MEA Recordings

The software MaxLab Live (MaxWell Biosystems [68]), was used to control and visualize the HD-MEA recordings. Therefore, all plated chips were sequentially connected to a MaxOne board, which in turn was connected to a Field Programmable Gate Array (FPGA), controlled by MaxLab installed on a computer. To map out spontaneous neuronal activity on the entire HD-MEA, seven dense block configurations, each recording 1'024 electrodes, were successively scanned through the electrode array. For every configuration, visible as colored areas in Fig. 2.3a, the activity was recorded for 120 seconds. After data was recorded, an algorithm identified amplitudes and spike times, on the measured electrodes which resulted in an activity map as displayed in Fig. 2.3b. The 1'024 electrodes with the most detected spikes were each routed to one readout channel, depicted as red squares in Fig. 2.3c. Therefore, electrode areas with no detectable or few spiking activities were excluded from further analysis. Following this electrode selection, we recorded the spontaneous electrical activity from this network for 10 minutes. Network activity of a more mature culture, recorded on all 1'024 channels, is plotted in Fig. 2.3d. Measurements started on the sixth or seventh day after cell plating and were repeated once a week.

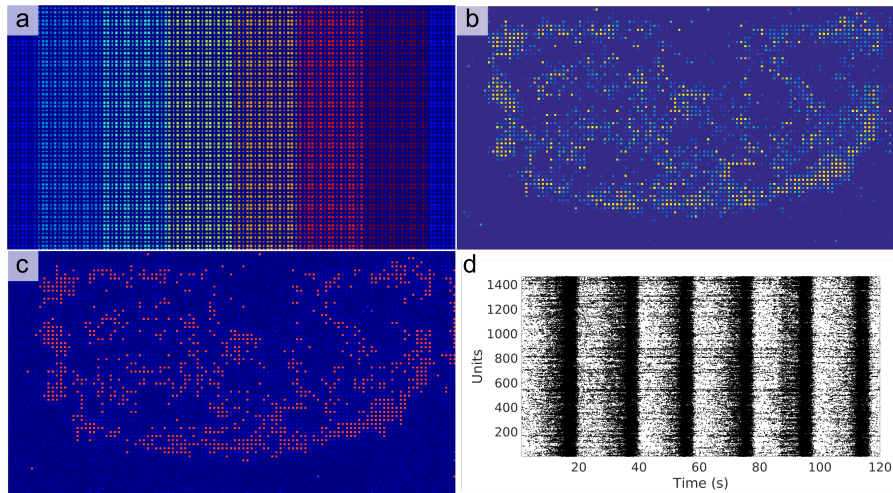


**Figure 2.3:** Modes and outputs of recordings. (a) Activity Scan of seven dense block configurations (colors) of 1'024 electrodes to cover all 26'400 electrodes. (b) Activity map of the activity scan screening the numbers of spikes recorded on each electrode as a color gradient from blue (less spike detection) to yellow (more spike detection). (c) 1'024 most suitable electrodes connected to readout channels to record a network scan. (d) Raster plot of spike activity read out by all channels.

### 2.2.2 Spike Sorting

Since the activity of a single neuron is usually detected on several fairly distant electrodes on a HD-MEA (see Fig. 2.4), it is difficult to keep apart signals of neurons lying close to each other. Hence, the obtained raw data must be pre-processed before evaluation and spiking activity assigned to individual neurons. This data processing is referred to as spike sorting.

Spike sorting the network recordings yields the spatial distribution of single cells, i.e. their “electrical footprints”. As an example, the spike-triggered average electrical footprint of three spike sorted units are depicted in Fig. 2.4a. Besides, Fig. 2.4b shows sixty milliseconds of raw data recorded on the five electrodes marked with arrows and



numbers in Fig. 2.4a. One can see, that at least two individual spikes can be identified on all five electrodes in this time period. However, the distinction of the recorded signals for neighboring neurons, such as the green, red and blue shapes, might be difficult on a single electrode based on temporal information only. Nevertheless, by further analyzing cumulative differences from various electrodes the activity of different cells can be differentiated.

The software package *spyking-circus* was used for spike sorting single cell activity [70]. Briefly, *spyking-circus* detects negative amplitude peaks of band-pass filtered data from different channels. For every spike recorded on an electrode, the signals were cut out, hereby referred to as templates. Depending on the position of the templates, all spikes having their maximum peak on the same electrode were divided into groups. For each group, the templates were then masked, assuming that a single cell can only influence electrodes nearby and only keeping those close to the peak electrode. As it is classically performed by many spike sorting algorithms, the templates were then projected into a lower dimensional feature space using principal component analysis (PCA) [71, 72]. Finally, all templates measured by different electrodes, yet belonging to the signal of the same neuron, referred to as a unit, are clustered together.

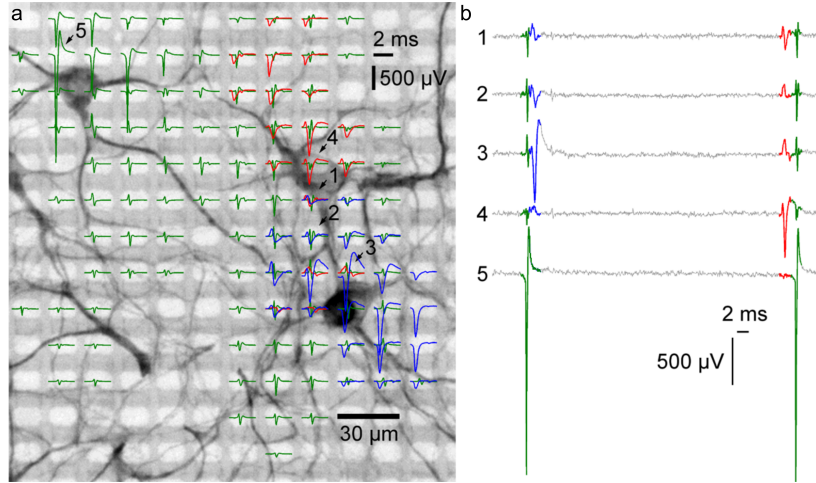


**Figure 2.4:** Electrical activity superimposed to staining of neurons plated on a HD-MEA. (a) The electrical activity of three neurons is superimposed to a fluorescence image of a MAP2 staining of the cell culture in the respective area. Spike-triggered averages of signals from 3 different neurons are drawn in green, red and blue. Averaged traces are only displayed for electrodes with a peak-to-peak signal amplitude exceeding a threshold of 50  $\mu\text{V}$ . The activity of a single cell can be recorded on several distant electrodes. (b) Sixty milliseconds of raw data recorded on the five electrodes marked with arrows and numbers in (a). At least two individual spikes can be identified in this period. Image taken from Müller *et al.* [59].

## 2.3 Data Analysis

In the present study, we analyzed the development of neuronal cultures over time (see Sec. 3.1.1 and Sec. 3.2.2) and the effect of different media compositions on spontaneous electrical activity (see Sec. 3.2.1). For the single cell- and network features we evaluated the spike sorted data, which provided multi-channel templates, storing spatial and temporal information. The code to analyze and plot the Results presented

in this chapter (see Ch. 3) was written in the multi-paradigm numerical computing environment MATLAB® R2019a and is attached to the appendix.

### 2.3.1 Single Cell Analysis

To characterize single cell spike waveform, we extracted firing rate, spike amplitude, amplitude half-width and axonal propagation velocity. We briefly explain each measure below:

**Firing Rate:** In order to calculate the firing rate of a unit, we divided the number of detected spikes by the duration of a recording.

**Spike Amplitude:** Next, we included the channel information of the corresponding templates to identify voltage values of every spike. We then extracted the averaged absolute peak values for the most dominant negative amplitude of each unit.

**Spike Half-Width:** Furthermore, by linear interpolation we computed the distance of the points left and right to the peak, at half maximum amplitude height, referred to as full width at half maximum.

**Axonal Propagation Velocity:** The propagation velocity of APs was calculated as the slope of the fit in a linear regression model of detected peaks, at distances normalized to the peak of the first recorded spike.

### 2.3.2 Network Analysis

To study the network dynamics of neuronal cultures, we binned the spike sorted activity over all detected neurons (1 ms bins) and studied their co-activity over time. A burst was defined as four times the standard deviation of co-active cells per time point.

**Co-Activity:** To obtain the percentage of co-active cells in a burst as a function of time, we divided the number of co-active cells by the total number of recorded units.

**Interburst Interval:** Interburst intervals provide a measure of the temporal regularity of activity among a culture. They were estimated as the average time period between two bursts.

**Burst Half-Width:** Moreover, we determined the full width at half maximum for every burst, to infer the average duration of the observed bursts.

### 2.3.3 Principal Component Analysis and Correlations

Clarification of differences in cellular- and network features across different time points, was obtained with PCA. Therefore, we converted correlations of every feature, evaluated among all cultures of a cell line, at every measured time point, into a two-dimensional graph. Clusters in this graph indicate highly correlated cell cultures. Besides, we created a graphical representation of correlations where the individual values contained in a matrix are represented as colors in order to display the strength of the linear relationship between single cell- and network features.

### 2.3.4 Repeated Measures Analysis of Variance

To probe differences across WT and A53T cultures and their development, we performed a repeated measures analysis of variance for every calculated single cell and network features. Therefore, we constructed a matrix for every investigated feature, containing the data for 16 cultures ( $n_{WT} = 9$ ,  $n_{A53T} = 7$ ) which survived from DIV 7 to DIV 28 and ran the analysis for the four time points. Each row of the matrix corresponds to a culture, each column corresponds to a time point. The degrees of freedom were  $(4-1) = 3$  for time,  $(4-1) \cdot (2-1) = 3$  for culture-time interaction and  $(16) \cdot (4-1) = 42$  for the error. Estimated p-values indicate the significance of the effect of time on the investigated features.

# 3

## Results

The results derived from the analysis of single cell spike waveforms and network activities of iPSC- and ESC-derived neuronal DA cultures are presented below. Initially this focuses on the electrophysiological characterization of iPSC-derived neuronal cultures (WT and A53T). These cells were tracked for four weeks with the goal of the first experimental series to identify the characteristics that could distinguish between WT and the disease type cultures (A53T)

Sec. 3.2 presents the results of our study of the effect of different culturing media compositions on spontaneous cellular activity (ESC-derived neurons) and the comparison of the electrical activity of a GBA1 gene knockout line (GBA1<sup>-/-</sup>) and a corresponding WT culture. The aim was to verify the media impact on spontaneous cell activity and to demonstrate the consequences of GBA1<sup>-/-</sup> on network creation.

### 3.1 iPSC-Derived Neurons

#### 3.1.1 Development of iPSC-Derived Neurons and Astrocytes

We investigated 10 WT- and 10 DT iPSC-derived cell cultures with the A53T mutation for 41 days, repeating the same electrophysiological recordings once a week. Fig. 3.1 illustrates the activity maps of one representative WT culture (upper panel) and the network activity (in Hz) recorded across 10 minutes during the corresponding network recording with the 1'024 most active electrodes.

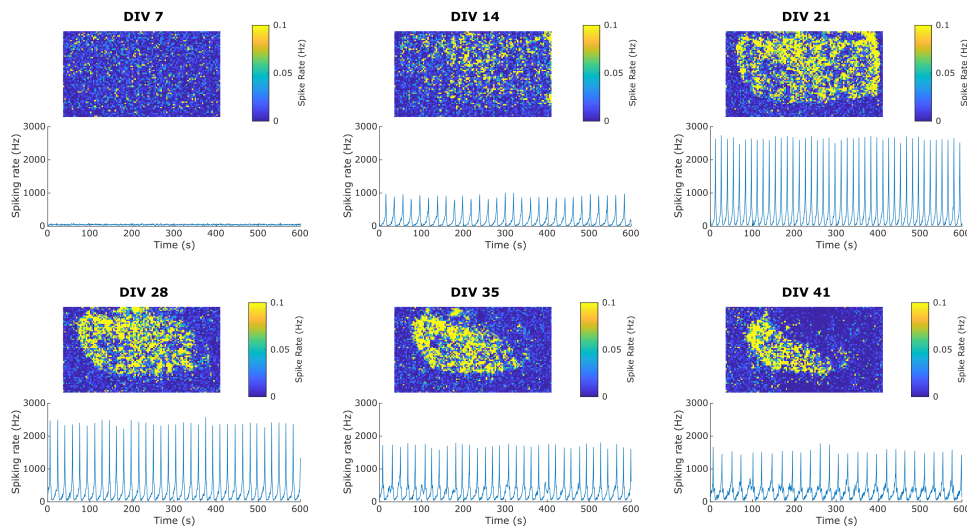


**Figure 3.1:** Six activity maps of a WT culture with corresponding spike numbers acquired during a network scan. Recordings were taken on DIV 7, 14, 21, 28, 35, and 41.

### 3.1.2 Single Cell Features

After spike sorting the raw data of all HD-MEA recordings, we analyzed changes of single cell features over time. Fig. 3.2 compares four features across four different instances (DIV 7, DIV 14, DIV 21 and DIV 28). Fig. 3.2a shows the average firing rate of every neuron from all WT and A53T cultures over time. The plot reveals an increase of single cell activity for both WT ( $0.37 \pm 0.08$  Hz -  $1.36 \pm 0.22$  Hz), where it reached a plateau ( $\sim$  DIV21), as well as for A53T ( $0.41 \pm 0.09$  Hz -  $1.30 \pm 0.25$  Hz) cultures. Fig. 3.2b likewise shows that the inferred amplitudes of extracellular AP wave forms for WT ( $37.44 \pm 1.14$   $\mu$ V -  $43.70 \pm 1.77$   $\mu$ V) and A53T ( $38.64 \pm 1.84$   $\mu$ V -  $45.63 \pm 1.45$   $\mu$ V) increased over time. Note, that we took the absolute value for these measurements as the extracellular APs have negative amplitudes. Fig. 3.2c shows the alteration of the full width at 50 % of the maximum extracellular AP amplitudes, which corresponds to the duration of a spike. There was again an increase over time, although the effect for WT cultures ( $0.257 \pm 0.002$  ms -  $0.271 \pm 0.004$  ms) was stronger compared to A53T ( $0.256 \pm 0.004$  ms -  $0.265 \pm 0.006$  ms). Panel d in Fig. 3.2 shows the development of AP propagation velocity. For the WT cultures the propagation velocity doubled in the first two weeks ( $0.49 \pm 0.11$  m/s -  $1.77 \pm 0.19$  m/s), whilst tripling for A53T cultures across the same time period ( $0.56 \pm 0.2$  m/s -  $1.75 \pm 0.29$  m/s). However, in both cases the propagation velocity saturated and remained constant after two weeks.

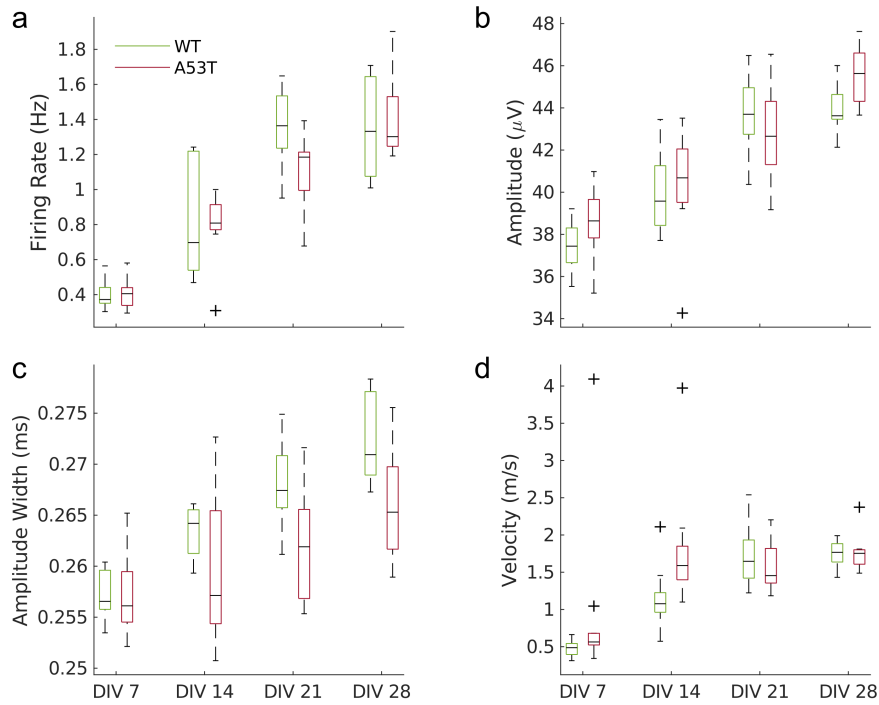


**Figure 3.2:** Comparison of single cell features between WT cultures (nDIV 7 = 10; nDIV 14 = 10; nDIV 21 = 9; nDIV 28 = 9) in green and A53T cultures (nDIV 7 = 10; nDIV 14 = 10; nDIV 21 = 9; nDIV 28 = 7) in red. Number of investigated cell cultures: (a) Averaged firing rates of single neurons as a function of age (DIV). (b) Absolute amplitude values as a function of age (DIV). (c) Spike half-width as a function of age (DIV). (d) AP propagation velocity as a function of age (DIV).

Fig. 3.3b shows the development of the most dominant negative waveform as the cell culture matured from DIV 7 to DIV 28. PCA of all WT cultures in Fig. 3.3c enabled

us to identify and subsequently cluster the cultures according to their age. There was also a correlation matrix of the analyzed waveform features of mature WT cultures on DIV 28 (3.3d), indicating that firing rate demonstrated a strong negative correlation to velocity and strongly with spike width. Furthermore, velocity and spike width were strongly correlated. A weak correlation was found with amplitude.

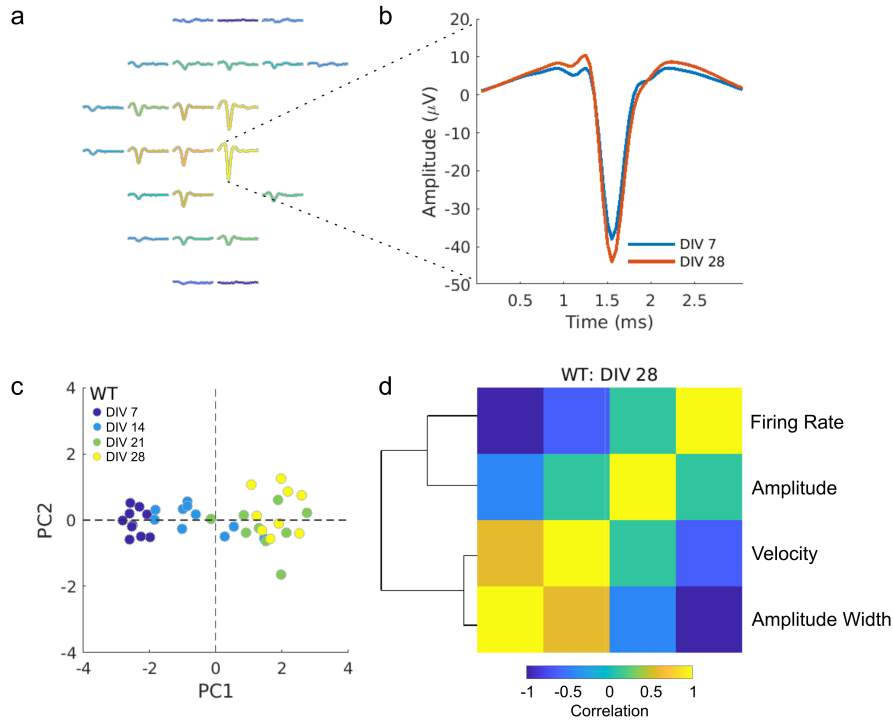


**Figure 3.3:** Distinctness of single cell features. (a) Neuronal footprint for a sorted unit after spike sorting. (b) Development of maximal Waveform over time (blue: DIV 7, red: DIV 28). (c) PCA of firing rate, amplitude, amplitude width and velocity from WT cultures clustered according to their age. (d) Correlation Matrix of single cell features indicating the strength of their linear relationship.

### 3.1.3 Network Features

In addition to single cell characterization, we also analyzed the development of neuronal network activities within the different cultures. Fig. 3.4 shows network features extracted from spontaneous burst behaviors, recorded across a four week period. As shown in Fig. 3.4a and b, we determined the number of simultaneously firing cells, recorded each millisecond at DIV 14 and 28 for WT and A53T cultures. The spontaneous co-activity revealed a neuronal burst pattern, increasing strongly during the first 2-3 weeks of development. Averaged durations of interburst intervals among WT and A53T cultures are plotted in Fig. 3.4c. Excluding the first week of activity, interburst intervals lasted approximately the same time at different ages ( $31.94 \pm 4.35$  s -  $34.97 \pm 5.72$  s for WT and  $30.03 \pm 9.81$  s -  $32.47 \pm 4.17$  s for A53T). Again excluding the first data points on DIV 7, Fig. 3.4d indicates that bursts lasted longer for WT than A53T - after two weeks a burst persisted for  $2.15 \pm 0.48$  s, while one week later the shortest burst time period was  $1.5 \pm 0.09$  s. For A53T cultures bursts lasted  $1.42 \pm 0.41$  s and  $1.23 \pm 0.21$  s respectively. The last plot in Fig. 3.4e represents the same feature as depicted in Fig. 3.4a and b, however for all recorded data sets across four

weeks. Unlike Fig. 3.4a and b, we normalized the data in Fig. 3.4e to the total number of units in a culture which revealed the percentage of co-active cells in a burst. For both cells co-activity increased with age, however the increase was larger for WT ( $\sim 0\% - 0.051 \pm 0.008\%$ ) than for A53T ( $0.002 \pm 0.005\% - 0.042 \pm 0.005\%$ ).

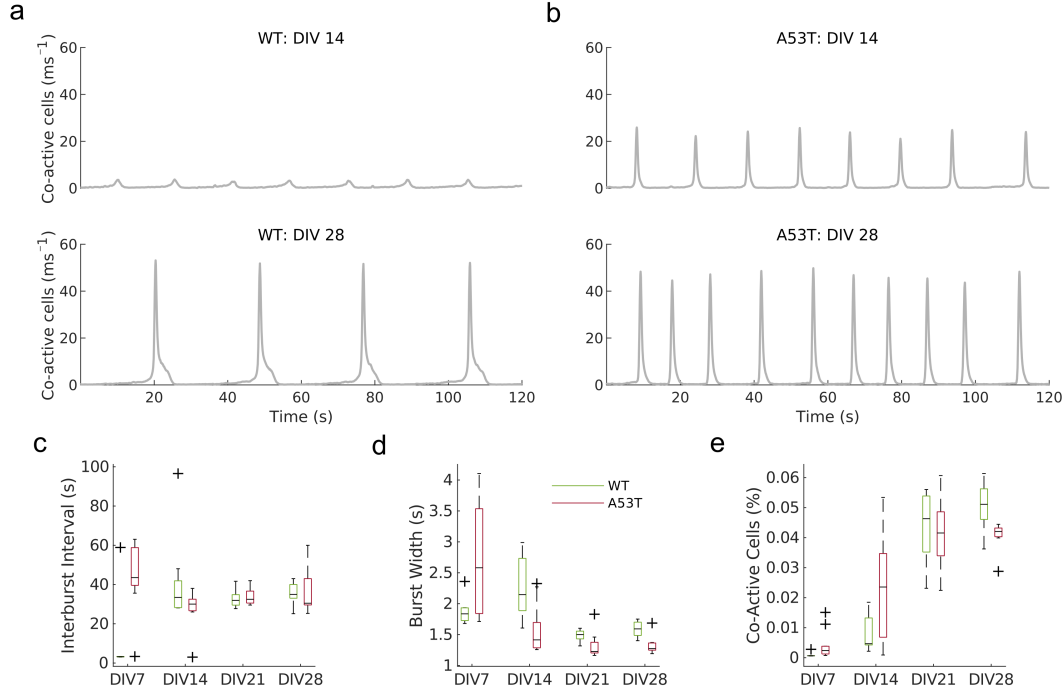


**Figure 3.4:** Comparison of network features between WT cultures ( $n_{\text{DIV } 7} = 10$ ;  $n_{\text{DIV } 14} = 10$ ;  $n_{\text{DIV } 21} = 9$ ;  $n_{\text{DIV } 28} = 9$ ) in green and A53T cultures ( $n_{\text{DIV } 7} = 10$ ;  $n_{\text{DIV } 14} = 10$ ;  $n_{\text{DIV } 21} = 9$ ;  $n_{\text{DIV } 28} = 7$ ) in red. (a) Co-active cells at DIV 14 (top) and DIV 28 (bottom) in WT culture as a function of time. (b) Co-active cells at DIV 14 (top) and DIV 28 (bottom) in A53T culture as a function of time. (c) Averaged interburst interval as a function of age (DIV). (d) Averaged burst width as a function of age (DIV). (e) Normalized percentage of co-active cells in a burst as a function of age (DIV).

Similarly to the single cell feature measurements, we performed a PCA on the evaluated network features and plotted the 1st and 2nd PCs – these are shown in Fig. 3.5a. With the exception of DIV 21 and 28, this allowed us to identify and cluster cultures according to their age. There was also a correlation matrix of the analyzed waveform features of mature WT cultures on DIV 28 in Fig. 3.5b indicating a strong anti-correlation of interburst interval with the other features. Burst width and co-activity have a positive correlation.

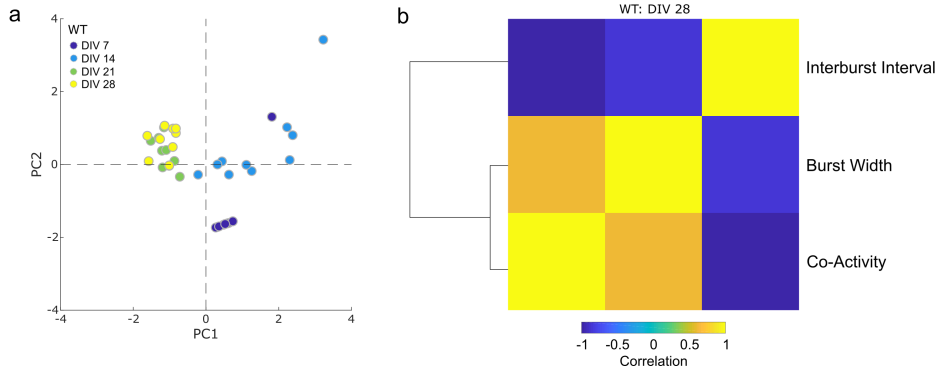


**Figure 3.5:** Distinctness of network features. (a) PCA of interburst interval, burst duration and co-active cells from WT cultures clustered according to their age. (b) Correlation Matrix of network features indicating the strength of their linear relationship.

### 3.1.4 Significance of Single Cell- and Network Features

**Firing Rate:** The firing rate was significantly different across the four days of measurement,  $F(3,3) = 85.06$ ,  $p < 0.001$ , however no significant difference in firing rate could be estimated between WT and A53T,  $F(3,3) = 0.85$ ,  $p > 0.05$ .

	<b>F</b>	<b>p-Value</b>
<b>DIV</b>	85.06	$6.99 \cdot 10^{-18}$
<b>Culture : DIV</b>	0.85	$4.74 \cdot 10^{-1}$

**Table 3.1:** Output of repeated measures analysis of variance for the firing rate. F indicates the value for the F-statistic and p its corresponding probability. A small p-value indicates significant term effect.

**AP Amplitude:** Amplitude was significantly different across the four days of measurement,  $F(3,3) = 69.16$ ,  $p < 0.001$ , however no significant difference in amplitude could be estimated between WT and A53T,  $F(3,3) = 0.99$ ,  $p > 0.05$ .

	<b>F</b>	<b>p-Value</b>
<b>DIV</b>	69.16	$2.71 \cdot 10^{-16}$
<b>Culture : DIV</b>	0.99	$4.09 \cdot 10^{-1}$

**Table 3.2:** Output of repeated measures analysis of variance for the AP amplitude. F indicates the value for the F-statistic and p its corresponding probability. A small p-value indicates significant term effect.

**Amplitude Width:** Amplitude width was significantly different across the four days of measurement,  $F(3,3) = 69.56$ ,  $p < 0.001$ , and we estimated a significant change in the amplitude width between WT and A53T,  $F(3,3) = 4.34$ ,  $p < 0.05$ .



	<b>F</b>	<b>p-Value</b>
<b>DIV</b>	69.56	$2.46 \cdot 10^{-16}$
<b>Culture : DIV</b>	4.34	$9.38 \cdot 10^{-3}$

**Table 3.3:** Output of repeated measure analysis of variance for the amplitude width. F indicates the value for the F-statistic and p its corresponding probability. A small p-value indicates a significant term effect.

**AP Propagation Velocity:** Velocity was significantly different across the four days of measurement,  $F(3,3) = 68.7$ ,  $p < 0.001$ . However no significant difference in velocity could be estimated between WT and A53T,  $F(3,3) = 1.73$ ,  $p > 0.05$ .

	<b>F</b>	<b>p-Value</b>
<b>DIV</b>	68.7	$3.05 \cdot 10^{-16}$
<b>Culture : DIV</b>	1.73	$1.75 \cdot 10^{-1}$

**Table 3.4:** Output of repeated measure analysis of variance for AP propagation velocity. F indicates the value for the F-statistic and p its corresponding probability. A small p-value indicates significant term effect.

**Co-Activity in Burst:** Co-activity was significantly different across the four days of measurement,  $F(3,3) = 156.35$ ,  $p < 0.001$ . Moreover, a significant difference was estimated for co-activity between WT and A53T,  $F(3,3) = 9.34$ ,  $p < 0.001$ .

	<b>F</b>	<b>p-Value</b>
<b>DIV</b>	156.35	$8.21 \cdot 10^{-23}$
<b>Culture : DIV</b>	9.34	$7.51 \cdot 10^{-5}$

**Table 3.5:** Output of repeated measure analysis of variance for the co-activity in a burst. F indicates the value for the F-statistic and p its corresponding probability. A small p-value indicates significant term effect.

**Interburst Interval:** Interburst intervals were significantly different across the four days of measurement,  $F(3,3) = 6.81$ ,  $p < 0.001$ , and furthermore, a significant difference in interburst intervals between WT and A53T was estimated,  $F(3,3) = 77.92$ ,  $p < 0.001$ .

	<b>F</b>	<b>p-Value</b>
<b>DIV</b>	6.81	$7.60 \cdot 10^{-4}$
<b>Culture : DIV</b>	77.92	$3.34 \cdot 10^{-17}$

**Table 3.6:** Output of repeated measure analysis of variance for the interburst interval. F indicates the value for the F-statistic and p its corresponding probability. A small p-value indicates significant term effect.

**Burst Duration:** Burst duration was significantly different across the four days of recording,  $F(3,3) = 45.72$ ,  $p < 0.001$  and we estimated a significant difference in burst duration between WT and A53T,  $F(3,3) = 34.53$ ,  $p < 0.001$ .

	<b>F</b>	<b>p-Value</b>
<b>DIV</b>	45.72	$2.73 \cdot 10^{-13}$
<b>Culture : DIV</b>	34.53	$2.06 \cdot 10^{-11}$

**Table 3.7:** Output of repeated measure analysis of variance for the burst duration. F indicates the value for the F-statistic and p its corresponding probability. A small p-value indicates significant term effect.

## 3.2 ESC-Derived Neurons

This section introduces the outcomes of the experiments performed with ESC-derived neurons provided by Professor Verdon Taylor (Department of Biomedicine, University of Basel). Initially, we tested the effect of culture medium composition on the electrical activity of ESC-derived neuronal cultures. In a second pilot experiment, we compared the electrical activity of WT- and GBA1<sup>-/-</sup> cultures across development.

### 3.2.1 Cell Culturing Media Effect

We analyzed 12 WT- and 12 DT ESC-derived neuronal cultures with GBA1<sup>-/-</sup> across 34 days, repeating activity- and network scan recordings once a week (as described for the iPSC experiments). Fig. 3.6 shows the activity maps of a GBA1<sup>-/-</sup> culture and spike numbers recorded for 10 minutes during each corresponding network scan with the 1'024 most active electrodes. In the first four weeks we cultured and measured the cells in NB-based medium, however up to DIV 20 almost no activity was detected. This is in strong contrast to the experiments with iPSC-derived neurons. At DIV 27, periodic activity patterns became visible in the plotted spike number and after recording we exchanged the medium to BP-based culturing medium. The network recording was repeated and a strong increase in electrical activity was observed.

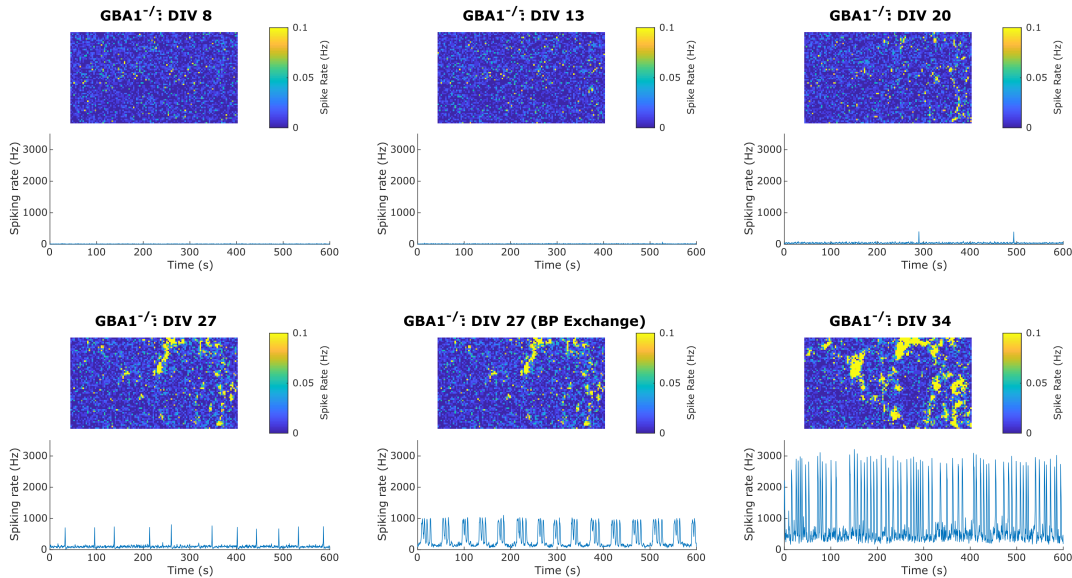


**Figure 3.6:** Six activity maps of a GBA1<sup>-/-</sup> culture with corresponding spike numbers acquired during a network scan. Recordings were taken on DIV 8, 13, 20, 27, and 34. NB-based medium was exchanged to BP-based medium on DIV 27.

### 3.2.2 Impact of $\text{GBA1}^{-/-}$ on Spontaneous Activity

In the third series of experiments, we analyzed 10 WT- and 10 DT ESC-derived neuronal  $\text{GBA1}^{-/-}$  cultures in BP-based medium across 20 days to study the impact on spontaneous electrical activity due to missing gene. As before, we repeated activity scans and network recordings every week. Fig. 3.7 compares the activity maps of WT- (Fig. 3.7a) and  $\text{GBA1}^{-/-}$  (Fig. 3.7b) cultures with corresponding spike numbers recorded for 10 minutes during a network scan of the 1'024 most active electrodes. The spontaneous activity of WT neuronal networks in Fig. 3.7a increased strongly across the 3 weeks of development. However,  $\text{GBA1}^{-/-}$  neuronal networks developed less electrical activity. For WT cultures about 15'000 spikes were detected in regular burst periods, while no burst pattern was seen for the barely active mutated cultures.

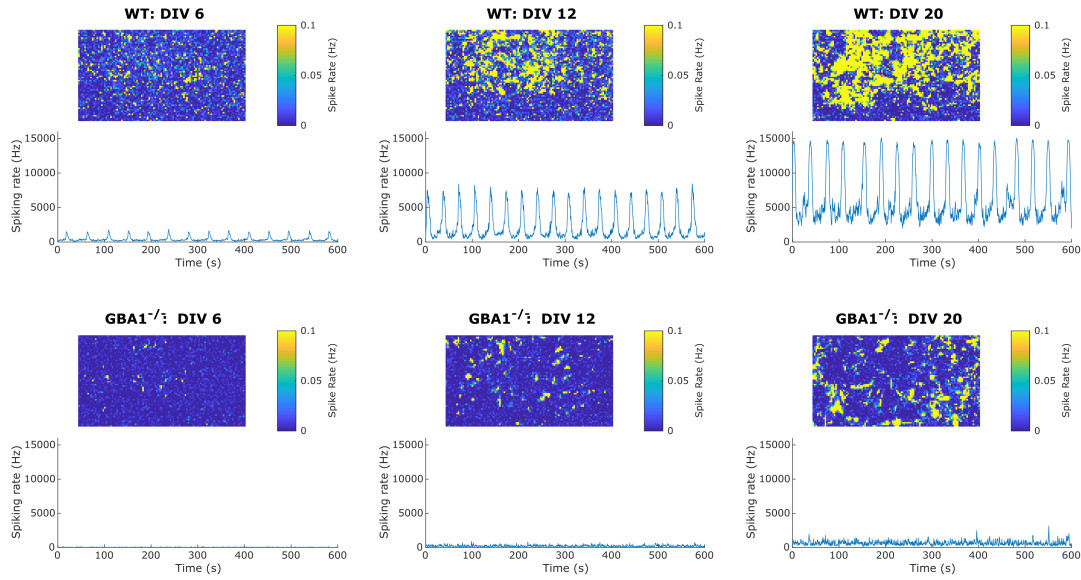


**Figure 3.7:** Three activity maps of a WT- (a) and a  $\text{GBA1}^{-/-}$  culture (b) with corresponding spike numbers acquired during a network scan. Recordings were taken on DIV 6, 12 and 20.

# 4

## Discussion

In this study, we applied state-of-the-art HD-MEAs to record human DA neuronal cultures. First, we studied the development of WT- and A53T iPSC-derived cells and showed that cells with the  $\alpha$ -syn mutation demonstrate an altered electrophysiological phenotype, both at the cellular and network level. In the second experiment, we studied the effect of cell medium on neuronal cell activity by comparing NB- and BP-based culturing media. In a final pilot study, we followed ESC-derived DA neuronal cultures over development and verified that cultures lacking GBA1<sup>-/-</sup> show a slowed maturity rate compared to healthy control cultures.

### 4.1 Defining the Neuronal Phenotype

For 41 days, we traced the culture development of isogenic iPSC-derived neuronal cell activity on HD-MEAs and compared among WT- and A53T cultures. In both cases a similar pattern was identified - cultures started to grow, and activity increased on the chip surface in the first 1-4 weeks.

Cellular features including firing rate, amplitude, amplitude width and velocity were inferred from the most pronounced spike waveform of the electrical footprint of individual spike sorted neurons (Fig. 3.3a and b). We analyzed the features over time and examined the differences among WT and A53T cell cultures. For firing rate, amplitude and amplitude width, the frequency shown in Fig. 3.2, voltage and distance respectively clearly increased with age for WT as well as for A53T. This effect was expected and demonstrates that cells matured on the HD-MEA. The axonal propagation velocity for both cell lines reached a plateau after DIV 21 and remained constant thereafter. The estimated average conduction velocities for WT (1.43 m/s - 1.99 m/s) and A53T (1.49 m/s - 2.37 m/s) at a mature stage at DIV 28 are at least 2-3 times faster than those reported for DA neurons in previous studies [73, 74, 75]. However, the values match those identified for non-DA neurons projecting to striatum, thalamus, or tectum [73, 74]. This naturally leads to the question whether a specification of > 80 % in WT- and A53T cultures is inappropriate, and hence our evaluations predominantly containing data of non-DA neurons negatively affected our results. Nevertheless, single cell features among a culture, illustrated for WT in Fig. 3.3c, could be ranked, and hence distinguished by age, by applying a PCA. Furthermore, the correlation matrix of mature WT cultures on DIV 28 in 3.3d revealed the strongest (although negative) correlation between firing rate and amplitude width, indicating that the AP of more frequently firing neurons have narrower amplitudes and vice versa. No correlations were found among firing rate and amplitude nor between velocity and amplitude, indicating that these features have little effect on each other. Additionally, the output

of repeated measure analysis of variance revealed that all single cell features significantly changed across development. Only spike half-width, however showed a significant difference between WT- and A53T cultures on a single day of measurement. As such, using only single cell features, it is hard to distinguish between A53T and WT cultures.

At the network level however, differences between the two lines became clearer. During the first week, burst patterns were detected in A53T cultures, in contrast at DIV 7 no bursts could be detected and almost no co-activity could be found in any WT culture (see Fig 3.4e), thus few interburst intervals were detected in Fig. 3.4c. Furthermore, Fig. 3.4a and b reveal at least three times greater co-activity for A53T in the second week. In turn, at DIV 28, both cultures reached about the same level of co-activity although the A53T burst pattern demonstrated more irregularities. Furthermore, burst width in Fig. 3.4d differed between cultures, lasting longer for WT cultures, however the burst duration estimated at DIV 7 for WT and A53T should be interpreted with caution - it was difficult to set a suitable threshold for burst detection at DIV 7 without affecting other recordings. Hence, in the first week, a large number of spike activities were detected as bursts even though no actual bursts occurred, which in turn falsified the data at the first recording day for WT- and led to large discrepancies in A53T cultures. This could be improved in future studies. The PCA in Fig. 3.5 indicated that measurements at DIV 21 and 28 were hard to distinguish - as the cluster of both recording days overlapped. However, network features at DIV 7 and 14 could be distinguished, with the exception of one outlier in each recording day. Moreover, the correlation matrix for the examined network features in Fig. 3.5b revealed a strong correlation among all three features. The strongest linear relationship was evaluated as a negative correlation between co-active cells and interburst intervals, predicting that many co-active cells in a culture generate more frequent bursts. Finally, repeated measure analysis of variance verified that all network features statistically differed depending on age and culture. Hence, it is possible to distinguish WT- and A53T cultures by analyzing features at the network level.

After 4 weeks of recording, activity started to decrease, perhaps indicating that the cultures were dying. The cause of death or inactivity is hard to deduce from HD-MEA recordings, as cell death may occur due to different reasons. During cell development on the chip, we observed cultures starting to cluster, as depicted in Fig. 3.1, which is in their nature [76]. However, such clusters easily detach from the electrode surface; thus these regions could not be recorded. Another reason may be due to exposure to unsterile environments while transporting cells to the measurement devices resulting in culture contamination -, the data at DIV 35 and 41 showed large discrepancies, potentially due to this and were excluded from further analysis.

## 4.2 Inhibitory- and Excitatory Effects of Culturing Media

In contrast to the commercially available iPSC-derived neurons, ESC-derived neurons provided by the lab of Professor Verdon Taylor (Fedele *et al.* in preparation), both WT as well as GBA1<sup>-/-</sup>, cultured in NB-based media, demonstrated almost no activity for up to three weeks (see Fig. 3.6). Only four out of 24 HD-MEA chips (1 WT and 3 GBA1<sup>-/-</sup>, all containing 30k cells/chip) showed a small amount of spiking activity at DIV 20. After DIV 27, the 20 still inactive chips were considered to be dead. The activity of four cultures that initially showed some activity, improved - yet only to a fraction of the activity normally observed for the iPSC-derived neurons. Interestingly however, exchanging the NB-based to BP-based medium instantly increased the spiking activity.

The inhibiting effect of NB, which was shown in a previous study, could be verified immediately after exchange (Fig. 3.6) DIV 27 (BP Exchange)) [77]. The number of recorded spikes after BP medium exchange was still only 1/3 of that detected in the iPSC development at DIV 28 (Fig. 3.1) in the first experimental series. Yet, the effect of BP-based medium was the same, since chip cultures in this second experimental series only contained 1/3 of the cell densities compared to those plated with iPSC-derived neurons.

### 4.3 GBA1 Affecting Network Creation

Experiments with ESC-derived GBA1/GBA1-knockout neuronal cultures with a plating density of 50k cells/chip in BP-based media, unveiled a distinguishable activity pattern between WT- and GBA1<sup>-/-</sup> cultures. In contrast to iPSC-derived neurons, shown in Fig. 3.7, WT cultures already generated bursts during the first week recording. Burst numbers increased drastically while age, implying that network formation within a culture already occurred at an early state. On the other hand, for GBA1<sup>-/-</sup> cultures only weak activities were recorded and even after three weeks no burst patterns were visible. This observed behavior coincides with an ongoing study, where it is shown that the GBA1<sup>-/-</sup> mutation evolve neurons with small soma sizes and shorter axonal extensions (Fedele *et al.* in preparation). These circumstances hinder network formation and network features, such as bursts, barely develop. Lastly, from the 20 plated chips in this experimental trial, only four WT cultures evolved strong activity with large discrepancy which complicated further statistical evaluations.

# 5

## Conclusion and Outlook

In summary, we used HD-MEA recordings to investigate the electrophysiological development of WT- and mutated human stem cell derived DA neurons. Results of this study provide further support for HD-MEAs as a reliable tool for stem cell experiments, allowing simultaneous recordings from various neurons at high spatial and temporal resolution. We concluded that single cell features, and in particular network features are valuable indicators of the phenotype in a neuronal culture. Evaluating features among different time points revealed whether cultures were healthy controls or carriers of the A53T mutation.

In addition, we verified inhibition of cell activity in human ESC-derived neurons due to NB-based culture media and rescued the negative effect by substituting cells into BP-based neuronal growth solution. Mapping culture activity demonstrated that the GBA1<sup>-/-</sup> mutation hinders formation of fully functional networks.

Although we were able to present a number of interesting differences between healthy and mutant cell lines, future work is required to elaborate these differences further. It is essential that iPSC cultures be verified to contain more than 80 % of DA neurons (as claimed by the vendor). If this proves untrue, it may have influenced the data collected in this study and could easily be tested by immunohistochemical staining for DA neurons. Additionally, the results would be easier to interpret if single DA neurons could be mapped out and followed. This could be achieved via optical stimulation of DA neurons and by viral transduction with targeted expression of humanized ChR2 in DA neurons. HD-MEA recordings of the stimulated activity in DA neurons would allow to parse out individual cells and allow recordings of their activity. Repeated measure analysis of variance only ascertains the significant distinction of at least two groups - to confirm the groups a post-hoc test needs to be calculated.

Despite this, combining human stem cell technology with HD-MEA recordings yields a state-of-the-art phenotypic screening platform, which will improve *in vitro* drug research, and lead to more personalized treatment strategies.

# A

## Appendix

In addition to the single cell- and network features studied in Sec. 3.1.2 and 3.1.3 respectively, we here introduce the codes for the plots written in MATLAB<sup>®</sup> R2019a.



---

```
clear;
close all;
warning off

%%%%%%%%%%%%%%%%%%%%%%%%%%%%%%%%%%%%%%%%%%%%%%%%%%%%%%%%%%%%%%%%%%%%%%%%%%%%%%
% Prepare Single Cell Data
%%%%%%%%%%%%%%%%%%%%%%%%%%%%%%%%%%%%%%%%%%%%%%%%%%%%%%%%%%%%%%%%%%%%%%%%%%%%%%

addpath(genpath('/home/prackg/Results/PDMEA/Codes/'));
data_path = '/home/prackg/Results/PDMEA/Archive/Analysis_Commercial/Single_Cell_Features/';
plot_path = '/home/prackg/Results/PDMEA/Archive/Analysis_Commercial/Figures/';

%%%%%%%%%%%%%%%%%%%%%%%%%%%%%%%%%%%%%%%%%%%%%%%%%%%%%%%%%%%%%%%%%%%%%%%%%%%%%%
% Load Data and Get Indices
%%%%%%%%%%%%%%%%%%%%%%%%%%%%%%%%%%%%%%%%%%%%%%%%%%%%%%%%%%%%%%%%%%%%%%%%%%%%%%

rate_WT_DIV07 = []; rate_WT_DIV14 = [];
rate_WT_DIV21 = []; rate_WT_DIV28 = [];

rate_PD_DIV07 = []; rate_PD_DIV14 = [];
rate_PD_DIV21 = []; rate_PD_DIV28 = [];

amp_WT_DIV07 = []; amp_WT_DIV14 = [];
amp_WT_DIV21 = []; amp_WT_DIV28 = [];

amp_PD_DIV07 = []; amp_PD_DIV14 = [];
amp_PD_DIV21 = []; amp_PD_DIV28 = [];

width_WT_DIV07 = []; width_WT_DIV14 = [];
width_WT_DIV21 = []; width_WT_DIV28 = [];

width_PD_DIV07 = []; width_PD_DIV14 = [];
width_PD_DIV21 = []; width_PD_DIV28 = [];

vel_WT_DIV07 = []; vel_WT_DIV14 = [];
vel_WT_DIV21 = []; vel_WT_DIV28 = [];

vel_PD_DIV07 = []; vel_PD_DIV14 = [];
vel_PD_DIV21 = []; vel_PD_DIV28 = [];

wave_WT_DIV07 = []; wave_WT_DIV14 = [];
wave_WT_DIV21 = []; wave_WT_DIV28 = [];

wave_PD_DIV07 = []; wave_PD_DIV14 = [];
wave_PD_DIV21 = []; wave_PD_DIV28 = [];

results_WT_DIV07 = dir(fullfile(data_path, '*WTSDS190314*'));
D7_index_WT = 1:length(results_WT_DIV07);
results_WT_DIV14 = dir(fullfile(data_path, '*WTSDS190321*'));
D14_index_WT = 1:length(results_WT_DIV14);
```

---

---

```

results_WT_DIV21 = dir(fullfile(data_path, '*WTSDS190328*'));
D21_index_WT = 1:length(results_WT_DIV21);
results_WT_DIV28 = dir(fullfile(data_path, '*WTSDS190404*'));
D28_index_WT = 1:length(results_WT_DIV28);

for a = 1:length(results_WT_DIV07)
    name = results_WT_DIV07(a).name;
    temp_path = [data_path name '/'];
    templates = dir(fullfile(temp_path, '*temp*'));
    cd(temp_path)

    mean_rate = []; mean_amp = []; mean_width = [];
    mean_vel = []; mean_wave = [];

    for b = 1:length(templates)
        load(templates(b).name);
        mean_rate = vertcat(mean_rate, table.rate);
        mean_amp = vertcat(mean_amp, table.amplitude);
        mean_width = vertcat(mean_width, table.halfwidth);

        if ~isempty(table.velocity)
            mean_vel = ...
                vertcat(mean_vel, table.velocity.Coefficients.Estimate);
        end

        mean_wave = horzcat(mean_wave, table.maxwave);

    end

    rate_WT_DIV07 = vertcat(rate_WT_DIV07, mean(mean_rate));
    amp_WT_DIV07 = vertcat(amp_WT_DIV07, mean(mean_amp));
    width_WT_DIV07 = vertcat(width_WT_DIV07, mean(mean_width));
    vel_WT_DIV07 = vertcat(vel_WT_DIV07, mean(mean_vel));

    wave_WT_DIV07 = horzcat(wave_WT_DIV07, mean(mean_wave, 2));
    wave_WT_DIV07 = mean(wave_WT_DIV07, 2);

    clear mean_rate
    clear mean_amp
    clear mean_width
    clear mean_vel
    clear mean_wave

end

for a = 1:length(results_WT_DIV14)
    name = results_WT_DIV14(a).name;
    temp_path = [data_path name '/'];
    templates = dir(fullfile(temp_path, '*temp*'));
    cd(temp_path)

    mean_rate = []; mean_amp = []; mean_width = [];
    mean_vel = []; mean_wave = [];

```

---

---

```

for b = 1:length(templates)
    load(templates(b).name);
    mean_rate = vertcat(mean_rate,table.rate);
    mean_amp = vertcat(mean_amp,table.amplitude);
    mean_width = vertcat(mean_width,table.halfwidth);

    if ~isempty(table.velocity)
        mean_vel =...
            vertcat(mean_vel,table.velocity.Coefficients.Estimate);
    end

    mean_wave = horzcat(mean_wave,table.maxwave);

end

rate_WT_DIV14 = vertcat(rate_WT_DIV14,mean(mean_rate));
amp_WT_DIV14 = vertcat(amp_WT_DIV14,mean(mean_amp));
width_WT_DIV14 = vertcat(width_WT_DIV14,mean(mean_width));
vel_WT_DIV14 = vertcat(vel_WT_DIV14,mean(mean_vel));

wave_WT_DIV14 = horzcat(wave_WT_DIV14,mean(mean_wave,2));
wave_WT_DIV14 = mean(wave_WT_DIV14,2);

clear mean_rate
clear mean_amp
clear mean_width
clear mean_vel
clear mean_wave

end

for a = 1:length(results_WT_DIV21)
    name = results_WT_DIV21(a).name;
    temp_path = [data_path name '/'];
    templates = dir(fullfile(temp_path, '*temp*'));
    cd(temp_path)

    mean_rate = []; mean_amp = []; mean_width = [];
    mean_vel = []; mean_wave = [];

    for b = 1:length(templates)
        load(templates(b).name);
        mean_rate = vertcat(mean_rate,table.rate);
        mean_amp = vertcat(mean_amp,table.amplitude);
        mean_width = vertcat(mean_width,table.halfwidth);

        if ~isempty(table.velocity)
            mean_vel =...
                vertcat(mean_vel,table.velocity.Coefficients.Estimate);
        end

        mean_wave = horzcat(mean_wave,table.maxwave);

    end

end

```

---

---

```

rate_WT_DIV21 = vertcat(rate_WT_DIV21,mean(mean_rate));
amp_WT_DIV21 = vertcat(amp_WT_DIV21,mean(mean_amp));
width_WT_DIV21 = vertcat(width_WT_DIV21,mean(mean_width));
vel_WT_DIV21 = vertcat(vel_WT_DIV21,mean(mean_vel));

wave_WT_DIV21 = horzcat(wave_WT_DIV21,mean(mean_wave,2));
wave_WT_DIV21 = mean(wave_WT_DIV21,2);

clear mean_rate
clear mean_amp
clear mean_width
clear mean_vel
clear mean_wave

end

for a = 1:length(results_WT_DIV28)
    name = results_WT_DIV28(a).name;
    temp_path = [data_path name '/'];
    templates = dir(fullfile(temp_path, '*temp*'));
    cd(temp_path)

    mean_rate = []; mean_amp = []; mean_width = [];
    mean_vel = []; mean_wave = [];

    for b = 1:length(templates)
        load(templates(b).name);
        mean_rate = vertcat(mean_rate,table.rate);
        mean_amp = vertcat(mean_amp,table.amplitude);
        mean_width = vertcat(mean_width,table.halfwidth);

        if ~isempty(table.velocity)
            mean_vel = ...
                vertcat(mean_vel,table.velocity.Coefficients.Estimate);
        end

        mean_wave = horzcat(mean_wave,table.maxwave);
    end

    rate_WT_DIV28 = vertcat(rate_WT_DIV28,mean(mean_rate));
    amp_WT_DIV28 = vertcat(amp_WT_DIV28,mean(mean_amp));
    width_WT_DIV28 = vertcat(width_WT_DIV28,mean(mean_width));
    vel_WT_DIV28 = vertcat(vel_WT_DIV28,mean(mean_vel));

    wave_WT_DIV28 = horzcat(wave_WT_DIV28,mean(mean_wave,2));
    wave_WT_DIV28 = mean(wave_WT_DIV28,2);

    clear mean_rate
    clear mean_amp
    clear mean_width
    clear mean_vel

```

---

---

```

clear mean_wave

end

results_PD_DIV07 = dir(fullfile(data_path, '*PDS190314*'));
D7_index_PD = 1:length(results_PD_DIV07);
results_PD_DIV14 = dir(fullfile(data_path, '*PDS190321*'));
D14_index_PD = 1:length(results_PD_DIV14);
results_PD_DIV21 = dir(fullfile(data_path, '*PDS190328*'));
D21_index_PD = 1:length(results_PD_DIV21);
results_PD_DIV28 = dir(fullfile(data_path, '*PDS190404*'));
D28_index_PD = 1:length(results_PD_DIV28);

for a = 1:length(results_PD_DIV07)
    name = results_PD_DIV07(a).name;
    temp_path = [data_path name '/'];
    templates = dir(fullfile(temp_path, '*temp*'));
    cd(temp_path)

    mean_rate = []; mean_amp = []; mean_width = [];
    mean_vel = []; mean_wave = [];

    for b = 1:length(templates)
        load(templates(b).name);
        mean_rate = vertcat(mean_rate, table.rate);
        mean_amp = vertcat(mean_amp, table.amplitude);
        mean_width = vertcat(mean_width, table.halfwidth);

        if ~isempty(table.velocity)
            mean_vel = ...
                vertcat(mean_vel, table.velocity.Coefficients.Estimate);
        end

        mean_wave = horzcat(mean_wave, table.maxwave);
    end

    rate_PD_DIV07 = vertcat(rate_PD_DIV07, mean(mean_rate));
    amp_PD_DIV07 = vertcat(amp_PD_DIV07, mean(mean_amp));
    width_PD_DIV07 = vertcat(width_PD_DIV07, mean(mean_width));
    vel_PD_DIV07 = vertcat(vel_PD_DIV07, mean(mean_vel));

    wave_PD_DIV07 = horzcat(wave_PD_DIV07, mean(mean_wave, 2));
    wave_PD_DIV07 = mean(wave_PD_DIV07, 2);

    clear mean_rate
    clear mean_amp
    clear mean_width
    clear mean_vel
    clear mean_wave

end

```

---

---

```

vel_PD_DIV07(10) = 0.5233;

for a = 1:length(results_PD_DIV14)
    name = results_PD_DIV14(a).name;
    temp_path = [data_path name '/'];
    templates = dir(fullfile(temp_path, '*temp*'));
    cd(temp_path)

    mean_rate = []; mean_amp = []; mean_width = [];
    mean_vel = []; mean_wave = [];

    for b = 1:length(templates)
        load(templates(b).name);
        mean_rate = vertcat(mean_rate, table.rate);
        mean_amp = vertcat(mean_amp, table.amplitude);
        mean_width = vertcat(mean_width, table.halfwidth);

        if ~isempty(table.velocity)
            mean_vel = ...
                vertcat(mean_vel, table.velocity.Coefficients.Estimate);
        end

        mean_wave = horzcat(mean_wave, table.maxwave);

    end

    rate_PD_DIV14 = vertcat(rate_PD_DIV14, mean(mean_rate));
    amp_PD_DIV14 = vertcat(amp_PD_DIV14, mean(mean_amp));
    width_PD_DIV14 = vertcat(width_PD_DIV14, mean(mean_width));
    vel_PD_DIV14 = vertcat(vel_PD_DIV14, mean(mean_vel));

    wave_PD_DIV14 = horzcat(wave_PD_DIV14, mean(mean_wave, 2));
    wave_PD_DIV14 = mean(wave_PD_DIV14, 2);

    clear mean_rate
    clear mean_amp
    clear mean_width
    clear mean_vel
    clear mean_wave

end

for a = 1:length(results_PD_DIV21)
    name = results_PD_DIV21(a).name;
    temp_path = [data_path name '/'];
    templates = dir(fullfile(temp_path, '*temp*'));
    cd(temp_path)

    mean_rate = []; mean_amp = []; mean_width = [];
    mean_vel = []; mean_wave = [];

    for b = 1:length(templates)
        load(templates(b).name);
        mean_rate = vertcat(mean_rate, table.rate);

```

---

---

```

    mean_amp = vertcat(mean_amp,table.amplitude);
    mean_width = vertcat(mean_width,table.halfwidth);

    if ~isempty(table.velocity)
        mean_vel = ...
            vertcat(mean_vel,table.velocity.Coefficients.Estimate);
    end

    mean_wave = horzcat(mean_wave,table.maxwave);

end

rate_PD_DIV21 = vertcat(rate_PD_DIV21,mean(mean_rate));
amp_PD_DIV21 = vertcat(amp_PD_DIV21,mean(mean_amp));
width_PD_DIV21 = vertcat(width_PD_DIV21,mean(mean_width));
vel_PD_DIV21 = vertcat(vel_PD_DIV21,mean(mean_vel));

wave_PD_DIV21 = horzcat(wave_PD_DIV21,mean(mean_wave,2));
wave_PD_DIV21 = mean(wave_PD_DIV21,2);

clear mean_rate
clear mean_amp
clear mean_width
clear mean_vel
clear mean_wave

end

for a = 1:length(results_PD_DIV28)
    name = results_PD_DIV28(a).name;
    temp_path = [data_path name '/'];
    templates = dir(fullfile(temp_path,'*temp*'));
    cd(temp_path)

    mean_rate = []; mean_amp = []; mean_width = [];
    mean_vel = []; mean_wave = [];

    for b = 1:length(templates)
        load(templates(b).name);
        mean_rate = vertcat(mean_rate,table.rate);
        mean_amp = vertcat(mean_amp,table.amplitude);
        mean_width = vertcat(mean_width,table.halfwidth);

        if ~isempty(table.velocity)
            mean_vel = ...
                vertcat(mean_vel,table.velocity.Coefficients.Estimate);
        end

        mean_wave = horzcat(mean_wave,table.maxwave);

    end

    rate_PD_DIV28 = vertcat(rate_PD_DIV28,mean(mean_rate));
    amp_PD_DIV28 = vertcat(amp_PD_DIV28,mean(mean_amp));

```

---

---

```

width_PD_DIV28 = vertcat(width_PD_DIV28,mean(mean_width));
vel_PD_DIV28 = vertcat(vel_PD_DIV28,mean(mean_vel));

wave_PD_DIV28 = horzcat(wave_PD_DIV28,mean(mean_wave,2));
wave_PD_DIV28 = mean(wave_PD_DIV28,2);

clear mean_rate
clear mean_amp
clear mean_width
clear mean_vel
clear mean_wave

end

cd(plot_path);

Rates = [rate_WT_DIV07;rate_PD_DIV07;rate_WT_DIV14;rate_PD_DIV14;...
         rate_WT_DIV21;rate_PD_DIV21;rate_WT_DIV28;rate_PD_DIV28];

g_rate = [ones(size(rate_WT_DIV07));2*ones(size(rate_PD_DIV07));...
          3*ones(size(rate_WT_DIV14));4*ones(size(rate_PD_DIV14));...
          5*ones(size(rate_WT_DIV21));6*ones(size(rate_PD_DIV21));...
          7*ones(size(rate_WT_DIV28));8*ones(size(rate_PD_DIV28))];

% Save .mat Files
save(['Rates' '.mat'],'Rates');
save(['g_rate' '.mat'],'g_rate');

Amplitudes = [amp_WT_DIV07;amp_PD_DIV07;...
              amp_WT_DIV14;amp_PD_DIV14;...
              amp_WT_DIV21;amp_PD_DIV21;...
              amp_WT_DIV28;amp_PD_DIV28];

g_amp = [ones(size(amp_WT_DIV07));2*ones(size(amp_PD_DIV07));...
          3*ones(size(amp_WT_DIV14));4*ones(size(amp_PD_DIV14));...
          5*ones(size(amp_WT_DIV21));6*ones(size(amp_PD_DIV21));...
          7*ones(size(amp_WT_DIV28));8*ones(size(amp_PD_DIV28))];

% Save .mat Files
save(['Amplitudes' '.mat'],'Amplitudes');
save(['g_amp' '.mat'],'g_amp');

Widths = [width_WT_DIV07;width_PD_DIV07;...
          width_WT_DIV14;width_PD_DIV14;...
          width_WT_DIV21;width_PD_DIV21;...
          width_WT_DIV28;width_PD_DIV28];

g_width = [ones(size(width_WT_DIV07));2*ones(size(width_PD_DIV07));...
            3*ones(size(width_WT_DIV14));4*ones(size(width_PD_DIV14));...
            5*ones(size(width_WT_DIV21));6*ones(size(width_PD_DIV21));...
            7*ones(size(width_WT_DIV28));8*ones(size(width_PD_DIV28))];

% Save .mat Files
save(['Widths' '.mat'],'Widths');

```

---



---

```

save(['g_width' '.mat'], 'g_width');

Velocities = [vel_WT_DIV07; vel_PD_DIV07; vel_WT_DIV14; vel_PD_DIV14; ...
    vel_WT_DIV21; vel_PD_DIV21; vel_WT_DIV28; vel_PD_DIV28];

g_vel = [ones(size(vel_WT_DIV07)); 2*ones(size(vel_PD_DIV07)); ...
    3*ones(size(vel_WT_DIV14)); 4*ones(size(vel_PD_DIV14)); ...
    5*ones(size(vel_WT_DIV21)); 6*ones(size(vel_PD_DIV21)); ...
    7*ones(size(vel_WT_DIV28)); 8*ones(size(vel_PD_DIV28))];

% Save .mat Files
save(['Velocities' '.mat'], 'Velocities');
save(['g_vel' '.mat'], 'g_vel');

Waves = [wave_WT_DIV07, wave_WT_DIV28];

% Save .mat Files
save(['Waves' '.mat'], 'Waves');

WT_mat_D07 = [rate_WT_DIV07, amp_WT_DIV07, ...
    width_WT_DIV07, vel_WT_DIV07];
WT_mat_D14 = [rate_WT_DIV14, amp_WT_DIV14, ...
    width_WT_DIV14, vel_WT_DIV14];
WT_mat_D21 = [rate_WT_DIV21, amp_WT_DIV21, ...
    width_WT_DIV21, vel_WT_DIV21];
WT_mat_D28 = [rate_WT_DIV28, amp_WT_DIV28, ...
    width_WT_DIV28, vel_WT_DIV28];

WT_mat = [WT_mat_D07(1:9,:), WT_mat_D14(1:9,:), WT_mat_D21, WT_mat_D28];

% Save .mat Files
save(['WT_mat' '.mat'], 'WT_mat');

WT_mat_D07_index = [ones(length(D7_index_WT), 1)*1, ...
    reshape(WT_mat_D07, length(D7_index_WT), [])];
WT_mat_D14_index = [ones(length(D14_index_WT), 1)*2, ...
    reshape(WT_mat_D14, length(D14_index_WT), [])];
WT_mat_D21_index = [ones(length(D21_index_WT), 1)*3, ...
    reshape(WT_mat_D21, length(D21_index_WT), [])];
WT_mat_D28_index = [ones(length(D28_index_WT), 1)*4, ...
    reshape(WT_mat_D28, length(D28_index_WT), [])];

WT_mat_combi = [WT_mat_D07_index; WT_mat_D14_index; ...
    WT_mat_D21_index; WT_mat_D28_index];

% Save .mat Files
save(['WT_mat_combi' '.mat'], 'WT_mat_combi');

PD_mat_D07 = [rate_PD_DIV07, amp_PD_DIV07, ...
    width_PD_DIV07, vel_PD_DIV07];
PD_mat_D14 = [rate_PD_DIV14, amp_PD_DIV14, ...
    width_PD_DIV14, vel_PD_DIV14];
PD_mat_D21 = [rate_PD_DIV21, amp_PD_DIV21, ...
    width_PD_DIV21, vel_PD_DIV21];

```

---

---

```

PD_mat_D28 = [rate_PD_DIV28, amp_PD_DIV28,...
              width_PD_DIV28, vel_PD_DIV28];

PD_mat = [PD_mat_D07(1:7,:),PD_mat_D14(1:7,:),...
          PD_mat_D21(1:7,:),PD_mat_D28];

% Save .mat Files
save(['PD_mat' '.mat'],'PD_mat');

PD_mat_D07_index = [ones(length(D7_index_PD),1)*1,...
                    reshape(PD_mat_D07, length(D7_index_PD), [])];
PD_mat_D14_index = [ones(length(D14_index_PD),1)*2,...
                    reshape(PD_mat_D14, length(D14_index_PD), [])];
PD_mat_D21_index = [ones(length(D21_index_PD),1)*3,...
                    reshape(PD_mat_D21, length(D21_index_PD), [])];
PD_mat_D28_index = [ones(length(D28_index_PD),1)*4,...
                    reshape(PD_mat_D28, length(D28_index_PD), [])];

PD_mat_combi = [PD_mat_D07_index; PD_mat_D14_index;...
               PD_mat_D21_index; PD_mat_D28_index];

% Save .mat Files
save(['PD_mat_combi' '.mat'],'PD_mat_combi');

% Get Dis-Similarity Between Cells
sim_vec = pdist(WT_mat_D28','correlation');
sim_mat = squareform(sim_vec);

% Average Linkage With Average Criteria
tree = linkage(sim_vec,'average');

% Find the Optimal Leaf Order (Group Most Similar Cells)
optimal_leafOrder = optimalleaforder(tree,sim_vec);

% Reorder Matrix
sim_mat_reordered = sim_mat(optimal_leafOrder,optimal_leafOrder);

%%%%%%%%%%%%%%%%%%%%%%%%%%%%%%%%%%%%%%%%%%%%%%%%%%%%%%%%%%%%%%%%%%%%%%%%
% Plot Figure 1
%%%%%%%%%%%%%%%%%%%%%%%%%%%%%%%%%%%%%%%%%%%%%%%%%%%%%%%%%%%%%%%%%%%%%%%%

Fig1 = figure('Position', [9 396 964 646],'color','white');

% Plot Spike Triggered Averages
cd '/home/prackg/Results/PDMEA/Archive/Data/Merged/DIV21/
PDSDS181214-2649/'
load unit-25.mat
sub8 = subplot(2,2,1);
plot_colored_template_circus(wfs_table.single_template_spatial,...
                             [wfs_table.x_inc wfs_table.y_inc],0,5);
axis square
axis tight

cd(plot_path);

```

---

---

```

% WT Wave Plot
sub1 = subplot(2,2,2);
sub1.Position = [0.47 0.5838 0.3347 0.3412];
ax1 = gca;
plot(Waves,'linev',2);
ylabel('Amplitude (\muV)');
legend({'DIV 7','DIV 28'},'Location','southeast');
legend boxoff;
axis square;
xticks([10 20 30 40 50]);
xlabel('Time (ms)');
xticklabels({'0.5','1','1.5','2','2.5'});
ax1.Box = 'off';

% PCA
sub2 = subplot(2,2,3);
ax2 = gca;
[coeff,score] = pca(zscore(WT_mat_combi(:,2:5)));
hold on;
h = scatter(score(:,1),score(:,2),20,WT_mat_combi(:,1),'filled');
h.MarkerEdgeColor = [0.7 0.7 0.7];
h.SizeData = 40;
set(gca, 'Box', 'off');
ylabel('PC2','FontSize',12);
xlabel('PC1','FontSize',12);
axis square
ax2.YTick = [-4 -2 0 2 4];
xlim([-4 4]);
ylim([-4 4]);
hold on;
plot([-5 5],[0 0],'--','Color',[0.2 0.2 0.2])
hold on;
plot([0 0],[-4 4],'--','Color',[0.2 0.2 0.2])
title1 = title('WT');
title1.FontWeight = 'normal';
title1.Position = [-3.8 3.5 0];
title1.HorizontalAlignment = 'left';

% Plot Dendrogram and Correlation Matrix
axes('Position',[0.44 0.145 0.1 0.27]);
h = dendrogram(tree,0,'reorder',optimal_leafOrder,...
    'Orientation','left','ColorThreshold',10); axis tight;axis off;
set(h,'Color',[0 0 0]);
box off
axes('Position',[0.47 0.1100 0.3347 0.3412]);
hold on; imagesc(1-sim_mat_reordered);
set(gca,'Box','off','TickDir','out','TickLength',[.0 .0],...
    'XMinorTick','off','YMinorTick','off','YGrid','off');
axis off;
axis square;
axis tight;
set(gca,'yticklabel',{[]});
xlabel('Metrics','FontSize',14);

```

---

---

```

title2 = title('WT: DIV 28');
title2.FontWeight = 'normal';

%%%%%%%%%%%%%%%%%%%%%%%%%%%%%%%%%%%%%%%%%%%%%%%%%%%%%%%%%%%%%%%%%%%%%%%%
% Figure 2
%%%%%%%%%%%%%%%%%%%%%%%%%%%%%%%%%%%%%%%%%%%%%%%%%%%%%%%%%%%%%%%%%%%%%%%%

Fig2 = figure('Position', [202 172 900 700], 'color', 'white');

% Boxplot Firing Rate
sub4 = subplot(2,2,1);
colors = [[0.4660 0.6740 0.1880];[0.6350 0.0780 0.1840]];
ax1 = gca;
boxplot(Rates,g_rate,'positions',...
        [1.25 1.75 3.25 3.75 5.25 5.75 7.25 7.75]);
med = findobj(gcf,'tag','Median');
set(med,'Color','k');
out = findobj(gcf,'tag','Outliers');
set(out,'MarkerEdgeColor','k');
box1 = findobj(gcf,'tag','Box');
box1(7).Color = colors(2,:);
box1(5).Color = colors(2,:);
box1(3).Color = colors(2,:);
box1(1).Color = colors(2,:);
box1(8).Color = colors(1,:);
box1(6).Color = colors(1,:);
box1(4).Color = colors(1,:);
box1(2).Color = colors(1,:);
uw = findobj(gcf,'tag','Upper Whisker');
set(uw,'LineStyle','--');
lw = findobj(gcf,'tag','Lower Whisker');
set(lw,'LineStyle','--');
ax1.XTickLabel = {};
ax1.XTick = [1.5 3.5 5.5 7.5];
ylabel('Firing Rate (Hz)');
axis square;
ax1.Box = 'off';
leg4 = legend([box1(8),box1(7)],{'WT','A53T'},...
              'Location','northwest','Box','off');

% Boxplot Amplitudes
sub5 = subplot(2,2,2);
sub5.Position(1) = 0.5;
colors = [[0.4660 0.6740 0.1880];[0.6350 0.0780 0.1840]];
ax5 = gca;
boxplot(Amplitudes,g_amp,'positions',...
        [1.25 1.75 3.25 3.75 5.25 5.75 7.25 7.75]);
med = findobj(gcf,'tag','Median');
set(med,'Color','k');
out = findobj(gcf,'tag','Outliers');
set(out,'MarkerEdgeColor','k');
box2 = findobj(gcf,'tag','Box');
box2(7).Color = colors(2,:);
box2(5).Color = colors(2,:);

```

---

---

```

box2(3).Color = colors(2,:);
box2(1).Color = colors(2,:);
box2(8).Color = colors(1,:);
box2(6).Color = colors(1,:);
box2(4).Color = colors(1,:);
box2(2).Color = colors(1,:);
uw = findobj(gcf,'tag','Upper Whisker');
set(uw,'LineStyle','--');
lw = findobj(gcf,'tag','Lower Whisker');
set(lw,'LineStyle','--');
ax5.XTickLabel = {};
ax5.XTick = [1.5 3.5 5.5 7.5];
ylabel('Amplitude (\muV)');
axis square;
ax5.Box = 'off';

% Boxplot Amplitude Half Mean Widths
sub6 = subplot(2,2,3);
sub6.Position(2) = 0.2;
colors = [[0.4660 0.6740 0.1880];[0.6350 0.0780 0.1840]];
ax6 = gca;
boxplot(Widths/20,g_width,'positions',...
    [1.25 1.75 3.25 3.75 5.25 5.75 7.25 7.75]);
med = findobj(gcf,'tag','Median');
set(med,'Color','k');
out = findobj(gcf,'tag','Outliers');
set(out,'MarkerEdgeColor','k');
box3 = findobj(gcf,'tag','Box');
box3(7).Color = colors(2,:);
box3(5).Color = colors(2,:);
box3(3).Color = colors(2,:);
box3(1).Color = colors(2,:);
box3(8).Color = colors(1,:);
box3(6).Color = colors(1,:);
box3(4).Color = colors(1,:);
box3(2).Color = colors(1,:);
uw = findobj(gcf,'tag','Upper Whisker');
set(uw,'LineStyle','--');
lw = findobj(gcf,'tag','Lower Whisker');
set(lw,'LineStyle','--');
ax6.XTickLabel = {'DIV 7','DIV 14','DIV 21','DIV 28'};
ax6.XTick = [1.5 3.5 5.5 7.5];
ylabel('Amplitude Width (ms)');
axis square;
ax6.Box = 'off';

% Boxplot AP propagation Velocity
sub7 = subplot(2,2,4);
sub7.Position(2) = 0.2;
sub7.Position(1) = 0.5;
colors = [[0.4660 0.6740 0.1880];[0.6350 0.0780 0.1840]];
ax7 = gca;
boxplot(Velocities,g_vel,'positions',...
    [1.25 1.75 3.25 3.75 5.25 5.75 7.25 7.75]);

```

---

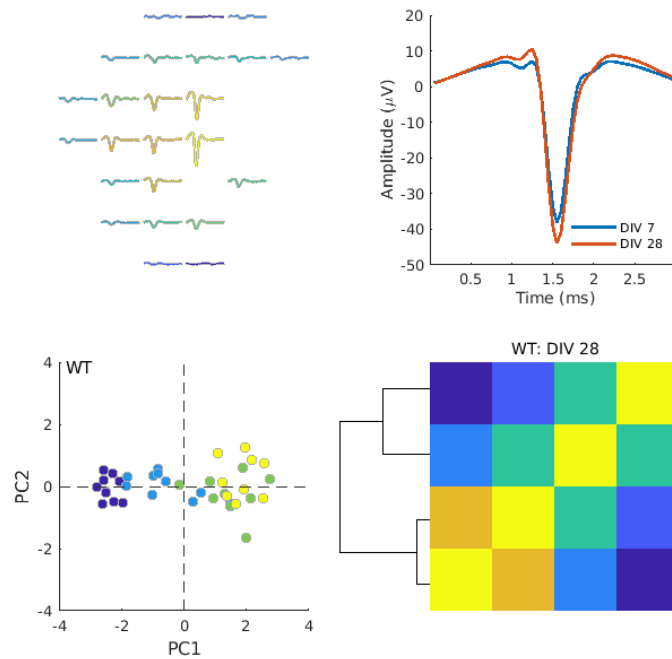
---

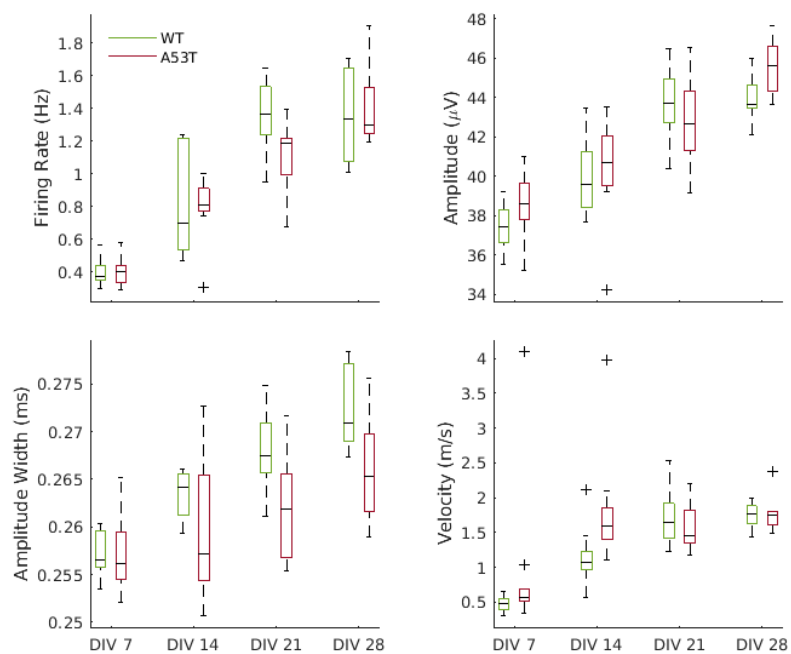
```

med = findobj(gcf,'tag','Median');
set(med,'Color','k');
out = findobj(gcf,'tag','Outliers');
set(out,'MarkerEdgeColor','k');
box4 = findobj(gcf,'tag','Box');
box4(7).Color = colors(2,:);
box4(5).Color = colors(2,:);
box4(3).Color = colors(2,:);
box4(1).Color = colors(2,:);
box4(8).Color = colors(1,:);
box4(6).Color = colors(1,:);
box4(4).Color = colors(1,:);
box4(2).Color = colors(1,:);
uw = findobj(gcf,'tag','Upper Whisker');
set(uw,'LineStyle','--');
lw = findobj(gcf,'tag','Lower Whisker');
set(lw,'LineStyle','--');
ax7.XTickLabel = {'DIV 7','DIV 14','DIV 21','DIV 28'};
ax7.XTick = [1.5 3.5 5.5 7.5];
ylabel('Velocity (m/s)');
axis square;
ax7.Box = 'off';

%Save
saveas(Fig1,'SingleCell11','png');
saveas(Fig1,'SingleCell11','svg');
saveas(Fig2,'SingleCell12','png');
saveas(Fig2,'SingleCell12','svg');

```





*Published with MATLAB® R2019a*

---

```
clear;
close all;
warning off

%%%%%%%%%%%%%%%%%%%%%%%%%%%%%%%%%%%%%%%%%%%%%%%%%%%%%%%%%%%%%%%%%%%%%%%%
% Prepare Network Data
%%%%%%%%%%%%%%%%%%%%%%%%%%%%%%%%%%%%%%%%%%%%%%%%%%%%%%%%%%%%%%%%%%%%%%%%

addpath(genpath('/home/prackg/Results/PDMEA/Codes/'));
data_path = '/home/prackg/Results/PDMEA/Archive/Analysis_Commercial/
Network_Features/';
plot_path = '/home/prackg/Results/PDMEA/Archive/Analysis_Commercial/
Figures/';

%%%%%%%%%%%%%%%%%%%%%%%%%%%%%%%%%%%%%%%%%%%%%%%%%%%%%%%%%%%%%%%%%%%%%%%%
% Load Data and get Indices
%%%%%%%%%%%%%%%%%%%%%%%%%%%%%%%%%%%%%%%%%%%%%%%%%%%%%%%%%%%%%%%%%%%%%%%%

burstrate_WT_DIV07 = []; burstrate_WT_DIV14 = [];
burstrate_WT_DIV21 = []; burstrate_WT_DIV28 = [];

burstrate_PD_DIV07 = []; burstrate_PD_DIV14 = [];
burstrate_PD_DIV21 = []; burstrate_PD_DIV28 = [];

dur_WT_DIV07 = []; dur_WT_DIV14 = [];
dur_WT_DIV21 = []; dur_WT_DIV28 = [];

dur_PD_DIV07 = []; dur_PD_DIV14 = [];
dur_PD_DIV21 = []; dur_PD_DIV28 = [];

co_WT_DIV07 = []; co_WT_DIV14 = [];
co_WT_DIV21 = []; co_WT_DIV28 = [];

co_PD_DIV07 = []; co_PD_DIV14 = [];
co_PD_DIV21 = []; co_PD_DIV28 = [];

cd(data_path)

load('WTSDS190314-2668.mat'); coact_WT_DIV07 = table.vec_smooth;
load('WTSDS190321-2668.mat'); coact_WT_DIV14 = table.vec_smooth;
load('WTSDS190328-2668.mat'); coact_WT_DIV21 = table.vec_smooth;
load('WTSDS190404-2668.mat'); coact_WT_DIV28 = table.vec_smooth;

load('PDSDS190314-2663.mat'); coact_PD_DIV07 = table.vec_smooth;
load('PDSDS190321-2663.mat'); coact_PD_DIV14 = table.vec_smooth;
load('PDSDS190328-2663.mat'); coact_PD_DIV21 = table.vec_smooth;
load('PDSDS190404-2663.mat'); coact_PD_DIV28 = table.vec_smooth;

results_WT_DIV07 = dir(fullfile(data_path, '*WTSDS190314*'));
D7_index_WT = 1:length(results_WT_DIV07);
results_WT_DIV14 = dir(fullfile(data_path, '*WTSDS190321*'));
D14_index_WT = 1:length(results_WT_DIV14);
```

---



---

```

results_WT_DIV21 = dir(fullfile(data_path, '*WTSDS190328*'));
D21_index_WT = 1:length(results_WT_DIV21);
results_WT_DIV28 = dir(fullfile(data_path, '*WTSDS190404*'));
D28_index_WT = 1:length(results_WT_DIV28);

for a = 1:length(results_WT_DIV07)
    name = results_WT_DIV07(a).name;
    load(name);
    burstrate_WT_DIV07 = ...
        vertcat(burstrate_WT_DIV07, mean(table.burstrate'));
    dur_WT_DIV07 = vertcat(dur_WT_DIV07, mean(table.burstwidth'));
    co_WT_DIV07 = vertcat(co_WT_DIV07, mean(table.burststamp'));
end

for a = 1:length(results_WT_DIV14)
    name = results_WT_DIV14(a).name;
    load(name);
    burstrate_WT_DIV14 = ...
        vertcat(burstrate_WT_DIV14, mean(table.burstrate'));
    dur_WT_DIV14 = vertcat(dur_WT_DIV14, mean(table.burstwidth'));
    co_WT_DIV14 = vertcat(co_WT_DIV14, mean(table.burststamp'));
end

for a = 1:length(results_WT_DIV21)
    name = results_WT_DIV21(a).name;
    load(name);
    burstrate_WT_DIV21 = ...
        vertcat(burstrate_WT_DIV21, mean(table.burstrate'));
    dur_WT_DIV21 = vertcat(dur_WT_DIV21, mean(table.burstwidth'));
    co_WT_DIV21 = vertcat(co_WT_DIV21, mean(table.burststamp'));
end

for a = 1:length(results_WT_DIV28)
    name = results_WT_DIV28(a).name;
    load(name);
    burstrate_WT_DIV28 = ...
        vertcat(burstrate_WT_DIV28, mean(table.burstrate'));
    dur_WT_DIV28 = vertcat(dur_WT_DIV28, mean(table.burstwidth'));
    co_WT_DIV28 = vertcat(co_WT_DIV28, mean(table.burststamp'));
end

results_PD_DIV07 = dir(fullfile(data_path, '*PDS190314*'));
D7_index_PD = 1:length(results_PD_DIV07);
results_PD_DIV14 = dir(fullfile(data_path, '*PDS190321*'));
D14_index_PD = 1:length(results_PD_DIV14);
results_PD_DIV21 = dir(fullfile(data_path, '*PDS190328*'));
D21_index_PD = 1:length(results_PD_DIV21);
results_PD_DIV28 = dir(fullfile(data_path, '*PDS190404*'));
D28_index_PD = 1:length(results_PD_DIV28);

for a = 1:length(results_PD_DIV07)

```

---

---

```

    name = results_PD_DIV07(a).name;
    load(name);
    burstrate_PD_DIV07 = ...
        vertcat(burstrate_PD_DIV07,mean(table.burstrate'));
    dur_PD_DIV07 = vertcat(dur_PD_DIV07,mean(table.burstwidth'));
    co_PD_DIV07 = vertcat(co_PD_DIV07,mean(table.burstamp'));

end

for a = 1:length(results_PD_DIV14)
    name = results_PD_DIV14(a).name;
    load(name);
    burstrate_PD_DIV14 = ...
        vertcat(burstrate_PD_DIV14,mean(table.burstrate'));
    dur_PD_DIV14 = vertcat(dur_PD_DIV14,mean(table.burstwidth'));
    co_PD_DIV14 = vertcat(co_PD_DIV14,mean(table.burstamp'));

end

for a = 1:length(results_PD_DIV21)
    name = results_PD_DIV21(a).name;
    load(name);
    burstrate_PD_DIV21 = ...
        vertcat(burstrate_PD_DIV21,mean(table.burstrate'));
    dur_PD_DIV21 = vertcat(dur_PD_DIV21,mean(table.burstwidth'));
    co_PD_DIV21 = vertcat(co_PD_DIV21,mean(table.burstamp'));

end

for a = 1:length(results_PD_DIV28)
    name = results_PD_DIV28(a).name;
    load(name);
    burstrate_PD_DIV28 = ...
        vertcat(burstrate_PD_DIV28,mean(table.burstrate'));
    dur_PD_DIV28 = vertcat(dur_PD_DIV28,mean(table.burstwidth'));
    co_PD_DIV28 = vertcat(co_PD_DIV28,mean(table.burstamp'));

end

cd(plot_path);

Burstrates = [burstrate_WT_DIV07;burstrate_PD_DIV07;...
    burstrate_WT_DIV14;burstrate_PD_DIV14;...
    burstrate_WT_DIV21;burstrate_PD_DIV21;...
    burstrate_WT_DIV28;burstrate_PD_DIV28];

g_burstrate = [ones(size(burstrate_WT_DIV07));...
    2*ones(size(burstrate_PD_DIV07));...
    3*ones(size(burstrate_WT_DIV14));...
    4*ones(size(burstrate_PD_DIV14));...
    5*ones(size(burstrate_WT_DIV21));...
    6*ones(size(burstrate_PD_DIV21));...
    7*ones(size(burstrate_WT_DIV28));...
    8*ones(size(burstrate_PD_DIV28))];

```

---

---

```

% Save .mat Files
save(['Burstrates' '.mat'], 'Burstrates');
save(['g_burstrate' '.mat'], 'g_burstrate');

Durations = [dur_WT_DIV07;dur_PD_DIV07;...
    dur_WT_DIV14;dur_PD_DIV14;...
    dur_WT_DIV21;dur_PD_DIV21;...
    dur_WT_DIV28;dur_PD_DIV28];

g_dur = [ones(size(dur_WT_DIV07));2*ones(size(dur_PD_DIV07));...
    3*ones(size(dur_WT_DIV14));4*ones(size(dur_PD_DIV14));...
    5*ones(size(dur_WT_DIV21));6*ones(size(dur_PD_DIV21));...
    7*ones(size(dur_WT_DIV28));8*ones(size(dur_PD_DIV28))];

% Save .mat Files
save(['Durations' '.mat'], 'Durations');
save(['g_dur' '.mat'], 'g_dur');

Coactivity = [co_WT_DIV07;co_PD_DIV07;co_WT_DIV14;co_PD_DIV14;...
    co_WT_DIV21;co_PD_DIV21;co_WT_DIV28;co_PD_DIV28];

g_co = [ones(size(co_WT_DIV07));2*ones(size(co_PD_DIV07));...
    3*ones(size(co_WT_DIV14));4*ones(size(co_PD_DIV14));...
    5*ones(size(co_WT_DIV21));6*ones(size(co_PD_DIV21));...
    7*ones(size(co_WT_DIV28));8*ones(size(co_PD_DIV28))];

% Save .mat Files
save(['Coactivity' '.mat'], 'Coactivity');
save(['g_co' '.mat'], 'g_co');

WT_mat_D07 = [burstrate_WT_DIV07, dur_WT_DIV07, co_WT_DIV07];
WT_mat_D14 = [burstrate_WT_DIV14, dur_WT_DIV14, co_WT_DIV14];
WT_mat_D21 = [burstrate_WT_DIV21, dur_WT_DIV21, co_WT_DIV21];
WT_mat_D28 = [burstrate_WT_DIV28, dur_WT_DIV28, co_WT_DIV28];

WT_mat_single = [WT_mat_D07(1:9,:), WT_mat_D14(1:9,:), ...
    WT_mat_D21, WT_mat_D28];

% Save .mat Files
save(['WT_mat_single' '.mat'], 'WT_mat_single');

WT_mat_D07_index = [ones(length(D7_index_WT),1)*1,...
    reshape(WT_mat_D07, length(D7_index_WT), [])];

WT_mat_D14_index = [ones(length(D14_index_WT),1)*2,...
    reshape(WT_mat_D14, length(D14_index_WT), [])];

WT_mat_D21_index = [ones(length(D21_index_WT),1)*3,...
    reshape(WT_mat_D21, length(D21_index_WT), [])];

WT_mat_D28_index = [ones(length(D28_index_WT),1)*4,...
    reshape(WT_mat_D28, length(D28_index_WT), [])];

```

---

---

```

WT_mat_combi_single = [WT_mat_D07_index; WT_mat_D14_index;...
    WT_mat_D21_index; WT_mat_D28_index];

% Save .mat Files
save(['WT_mat_combi_single' '.mat'], 'WT_mat_combi_single');

PD_mat_D07 = [burstrate_PD_DIV07, dur_PD_DIV07, co_PD_DIV07];
PD_mat_D14 = [burstrate_PD_DIV14, dur_PD_DIV14, co_PD_DIV14];
PD_mat_D21 = [burstrate_PD_DIV21, dur_PD_DIV21, co_PD_DIV21];
PD_mat_D28 = [burstrate_PD_DIV28, dur_PD_DIV28, co_PD_DIV28];

PD_mat = [PD_mat_D07(1:7,:), PD_mat_D14(1:7,:), ...
    PD_mat_D21(1:7,:), PD_mat_D28];

% Save .mat Files
save(['PD_mat' '.mat'], 'PD_mat');

PD_mat_D07_index = [ones(length(D7_index_PD),1)*1,...
    reshape(PD_mat_D07, length(D7_index_PD), [])];

PD_mat_D14_index = [ones(length(D14_index_PD),1)*2,...
    reshape(PD_mat_D14, length(D14_index_PD), [])];

PD_mat_D21_index = [ones(length(D21_index_PD),1)*3,...
    reshape(PD_mat_D21, length(D21_index_PD), [])];

PD_mat_D28_index = [ones(length(D28_index_PD),1)*4,...
    reshape(PD_mat_D28, length(D28_index_PD), [])];

PD_mat_combi = [PD_mat_D07_index; PD_mat_D14_index;...
    PD_mat_D21_index; PD_mat_D28_index];

% Save .mat Files
save(['PD_mat_combi' '.mat'], 'PD_mat_combi');

% Get Dis-Similarity between Cells
sim_vec = pdist(WT_mat_D28, 'correlation');
sim_mat = squareform(sim_vec);

% Average Linkage with Average Criteria
tree = linkage(sim_vec, 'average');

% Find the Optimal Leaf Order (Group Most Similar Cells)
optimal_leafOrder = optimallleaforder(tree, sim_vec);

% Reorder Matrix
sim_mat_reordered = sim_mat(optimal_leafOrder, optimal_leafOrder);

%%%%%%%%%%%%%%%%%%%%%%%%%%%%%%%%%%%%%%%%%%%%%%%%%%%%%%%%%%%%%%%%%%%%%%%%%%%%%%
% Plot data Figure 1
%%%%%%%%%%%%%%%%%%%%%%%%%%%%%%%%%%%%%%%%%%%%%%%%%%%%%%%%%%%%%%%%%%%%%%%%%%%%%%

Fig1 = figure('Position', [50 300 1000 750], 'color', 'white');

```

---

---

```

% Plot Smoothed Burst Vector
sub1 = subplot(3,3,[1 1.5]);
sub1.Position(4) = 0.15;
plot(smooth(coact_WT_DIV14,500), 'Color',[0.7 0.7 0.7], 'linew',1.3);
ax1 = gca;
axis tight
ylabel('Co-active cells (ms^{#1})');
ax1.XTickLabel = {};
xlim([1 120000]);
ylim([0 60]);
ax1.Box = 'off';
ax1.XAxis.Visible = 'off';
title1 = title('WT: DIV 14');
title1.Position(2) = 60;
title1.FontWeight = 'normal';

% Plot Smoothed Burst Vector
sub2 = subplot(3,3,[4 4.5]);
sub2.Position(4) = 0.15;
sub2.Position(2) = 0.5;
ax2 = gca;
plot(smooth(coact_WT_DIV28,500), 'Color',[0.7 0.7 0.7], 'linew',1.3);
axis tight
xlabel('Time (s)');
ylabel('Co-active cells (ms^{#1})');
ax2.XTick = [2*10^4 4*10^4 6*10^4 8*10^4 10*10^4 12*10^4];
ax2.XTickLabel = {'20','40','60','80','100','120'};
xlim([1 120000]);
ylim([0 60]);
ax2.Box = 'off';
title2 = title('WT: DIV 28');
title2.Position(2) = 60;
title2.FontWeight = 'normal';

% Plot Smoothed Burst Vector
sub3 = subplot(3,3,[2.5 3]);
sub3.Position(4) = 0.15;
ax3 = gca;
plot(smooth(coact_PD_DIV14,500), 'Color',[0.7 0.7 0.7], 'linew',1.3);
axis tight
xticks([]);
ax3.XTickLabel = {};
xlim([1 120000]);
ylim([0 60]);
ax3.Box = 'off';
ax3.XAxis.Visible = 'off';
title3 = title('A53T: DIV 14');
title3.Position(2) = 60;
title3.FontWeight = 'normal';

% Plot Smoothed Burst Vector
sub4 = subplot(3,3,[5.5 6]);
sub4.Position(4) = 0.15;
sub4.Position(2) = 0.5;

```

---

---

```

ax4 = gca;
plot(smooth(coact_PD_DIV28,500), 'Color',[0.7 0.7 0.7], 'linew',1.3);
axis tight
xlabel('Time (s)');
ax4.XTick = [2*10^4 4*10^4 6*10^4 8*10^4 10*10^4 12*10^4];
ax4.XTickLabel = {'20','40','60','80','100','120'};
xlim([1 120000]);
ylim([0 60]);
ax4.Box = 'off';
title4 = title('A53T: DIV 28');
title4.Position(2) = 60;
title4.FontWeight = 'normal';

% Boxplot Firing Rate
sub5 = subplot(3,3,7);
sub5.Position(2) = 0.2;
ax5 = gca;
colors = [[0.4660 0.6740 0.1880];[0.6350 0.0780 0.1840]];
boxplot(Burstrates,g_burstrate,'positions',...
    [1.25 1.75 3.25 3.75 5.25 5.75 7.25 7.75]);
med = findobj(gcf,'tag','Median');
set(med,'Color','k');
out = findobj(gcf,'tag','Outliers');
set(out,'MarkerEdgeColor','k');
boxl = findobj(gcf,'tag','Box');
boxl(7).Color = colors(2,:);
boxl(5).Color = colors(2,:);
boxl(3).Color = colors(2,:);
boxl(1).Color = colors(2,:);
boxl(8).Color = colors(1,:);
boxl(6).Color = colors(1,:);
boxl(4).Color = colors(1,:);
boxl(2).Color = colors(1,:);
uw = findobj(gcf,'tag','Upper Whisker');
set(uw,'LineStyle','--');
lw = findobj(gcf,'tag','Lower Whisker');
set(lw,'LineStyle','--');
ax5.XTickLabel = {'DIV7','DIV14','DIV21','DIV28'};
ax5.XTick = [1.5 3.5 5.5 7.5];
ylabel('Interburst Interval (s)');
axis square;
ax5.Box = 'off';

% Boxplot Amplitude Half Mean Widths
sub6 = subplot(3,3,8);
sub6.Position(2) = 0.2;
ax6 = gca;
colors = [[0.4660 0.6740 0.1880];[0.6350 0.0780 0.1840]];
boxplot(Durations,g_dur,'positions',...
    [1.25 1.75 3.25 3.75 5.25 5.75 7.25 7.75]);
med = findobj(gcf,'tag','Median');
set(med,'Color','k');
out = findobj(gcf,'tag','Outliers');
set(out,'MarkerEdgeColor','k');

```

---

---

```

box2 = findobj(gcf,'tag','Box');
box2(7).Color = colors(2,:);
box2(5).Color = colors(2,:);
box2(3).Color = colors(2,:);
box2(1).Color = colors(2,:);
box2(8).Color = colors(1,:);
box2(6).Color = colors(1,:);
box2(4).Color = colors(1,:);
box2(2).Color = colors(1,:);
uw = findobj(gcf,'tag','Upper Whisker');
set(uw,'LineStyle','--');
lw = findobj(gcf,'tag','Lower Whisker');
set(lw,'LineStyle','--');
ax6.XTickLabel = {'DIV7','DIV14','DIV21','DIV28'};
ax6.XTick = [1.5 3.5 5.5 7.5];
axis square;
ylabel('Burst Width (s)');
ax6.Box = 'off';
legend([box2(8),box2(7)],{'WT','A53T'},'Location',...
        'northeast','Box','off');

% Boxplot Co-Activity
sub7 = subplot(3,3,9);
sub7.Position(2) = 0.2;
ax7 = gca;
colors = [[0.4660 0.6740 0.1880];[0.6350 0.0780 0.1840]];
boxplot(Coactivity,g_co,'positions',...
        [1.25 1.75 3.25 3.75 5.25 5.75 7.25 7.75]);
med = findobj(gcf,'tag','Median');
set(med,'Color','k');
out = findobj(gcf,'tag','Outliers');
set(out,'MarkerEdgeColor','k');
box3 = findobj(gcf,'tag','Box');
box3(7).Color = colors(2,:);
box3(5).Color = colors(2,:);
box3(3).Color = colors(2,:);
box3(1).Color = colors(2,:);
box3(8).Color = colors(1,:);
box3(6).Color = colors(1,:);
box3(4).Color = colors(1,:);
box3(2).Color = colors(1,:);
uw = findobj(gcf,'tag','Upper Whisker');
set(uw,'LineStyle','--');
lw = findobj(gcf,'tag','Lower Whisker');
set(lw,'LineStyle','--');
ax7.XTickLabel = {'DIV7','DIV14','DIV21','DIV28'};
ax7.XTick = [1.5 3.5 5.5 7.5];
axis square;
ylabel('Co-Active Cells (%)');
ax7.Box = 'off';

%%%%%%%%%%%%%%%%%%%%%%%%%%%%%%%%%%%%%%%%%%%%%%%%%%%%%%%%%%%%%%%%%%%%%%%%%%%%%%
% Plot Figure 2
%%%%%%%%%%%%%%%%%%%%%%%%%%%%%%%%%%%%%%%%%%%%%%%%%%%%%%%%%%%%%%%%%%%%%%%%%%%%%%

```

---

---

```

Fig2 = figure('Position', [50 622 1599 428], 'color', 'white');

% PCA
sub8 = subplot(1,2,1);
ax8 = gca;
[coeff,score] = pca(zscore(WT_mat_combi_single(:,2:4)));
hold on;
h = scatter(score(:,1),score(:,2),20,...
    WT_mat_combi_single(:,1),'filled');
h.MarkerEdgeColor = [0.7 0.7 0.7];
h.SizeData = 40;
set(gca, 'Box', 'off');
ylabel('PC2','FontSize',12);
xlabel('PC1','FontSize',12);
axis square
ax8.YTick = [-4 -2 0 2 4];
xlim([-4 4]);
ylim([-4 4]);
hold on;
plot([-5 5],[0 0],'--','Color',[0.2 0.2 0.2])
hold on;
plot([0 0],[-4 4],'--','Color',[0.2 0.2 0.2])
title1 = title('WT');
title1.FontWeight = 'normal';
title1.Position = [-3.8 3.5 0];
title1.HorizontalAlignment = 'left';

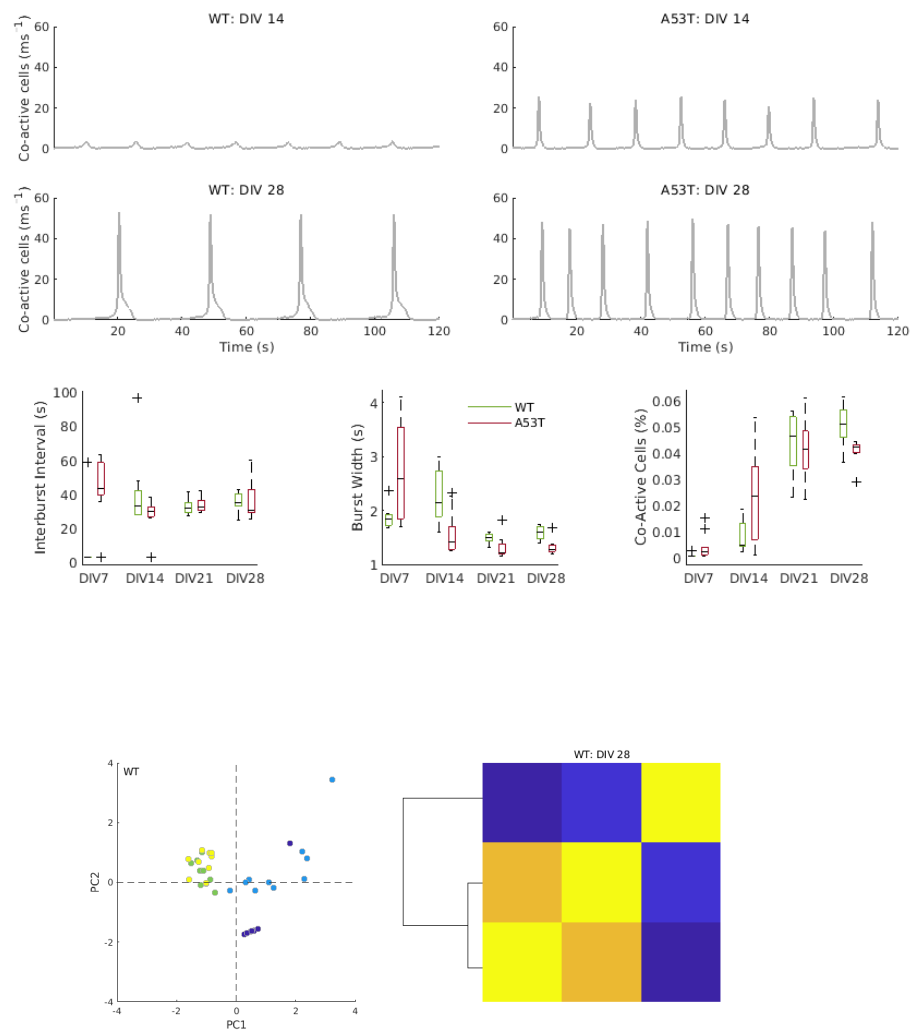
% Plot Dendrogram and Correlation Matrix
axes('Position',[0.45 0.225 0.075 0.58]);
h = dendrogram(tree,0,'reorder',optimal_leafOrder,...
    'Orientation','left','ColorThreshold',10);...
    axis tight; axis off;
set(h,'Color',[0 0 0]);
box off
axes('Position',[0.465 0.1100 0.3347 0.8150]);
hold on; imagesc(1-sim_mat_reordered);
set(gca,'Box','off','TickDir','out','TickLength',[.0 .0],...
    'XMinorTick','off','YMinorTick','off','YGrid','off');
axis off;
axis square;
axis tight;
set(gca,'yticklabel',{[]});
xlabel('Metrics','FontSize',14);
title2 = title('WT: DIV 28');
title2.FontWeight = 'normal';

%Save
saveas(Fig1,'Network1','png');
saveas(Fig1,'Network1','svg');
saveas(Fig2,'Network2','png');
saveas(Fig2,'Network2','svg');

```

---





Published with MATLAB® R2019a

# References

- [1] Aparna R Desai and Susan K McConnell. "Progressive Restriction in Fate Potential by Neural Progenitors During Cerebral Cortical Development". In: *Development* 127.13 (2000), pp. 2863–2872.
- [2] Xueming Qian et al. "Timing of CNS Cell Generation: A Programmed Sequence of Neuron and Glial Cell Production from Isolated Murine Cortical Stem Cells". In: *Neuron* 28.1 (2000), pp. 69–80.
- [3] WA Harris. "Temporal Coordinates: The Genes that Fix Cell Fate with Birth Order". In: *Developmental Cell* 1.3 (2001), pp. 313–314.
- [4] Santiago Ramón y Cajal. *The Neuron and the Glial Cell*. Charles C Thomas Pub Ltd, 1984.
- [5] Santiago Ramón y Cajal. *New Ideas on the Structure of the Nervous System in Man and Vertebrates*. MIT Press, 1990.
- [6] Klaus-Armin Nave. "Myelination and Support of Axonal Integrity by Glia". In: *Nature* 468.7321 (2010), p. 244.
- [7] Masaki Ueno et al. "Layer V Cortical Neurons Require Microglial Support for Survival during Postnatal Development". In: *Nature Neuroscience* 16.5 (2013), p. 543.
- [8] Fiona Doetsch. "The Glial Identity of Neural Stem Cells". In: *Nature neuroscience* 6.11 (2003), p. 1127.
- [9] Arnold Kriegstein and Arturo Alvarez-Buylla. "The Glial Nature of Embryonic and Adult Neural Stem Cells". In: *Annual Review of Neuroscience* 32 (2009), pp. 149–184.
- [10] Almudena Ramón-Cueto et al. "Functional Recovery of Paraplegic Rats and Motor Axon Regeneration in Their Spinal Cords by Olfactory Ensheathing Glia". In: *Neuron* 25.2 (2000), pp. 425–435.
- [11] JL Ridet et al. "Reactive Astrocytes: Cellular and Molecular Cues to Biological Function". In: *Trends in Neurosciences* 20.12 (1997), pp. 570–577.
- [12] RD Keynes. "The Ionic Movements During Nervous Activity". In: *The Journal of Physiology* 114.1-2 (1951), pp. 119–150.
- [13] Alan Lloyd Hodgkin. "The Croonian Lecture: Ionic Movements and Electrical Activity in Giant Nerve Fibres". In: *Proc. R. Soc. Lond. B* 148.930 (1958), pp. 1–37.
- [14] Jian-Kang Zhu. "Regulation of Ion Homeostasis under Salt Stress". In: *Current Opinion in Plant Biology* 6.5 (2003), pp. 441–445.
- [15] Raymond Dingledine et al. "The Glutamate Receptor Ion Channels". In: *Pharmacological Reviews* 51.1 (1999), pp. 7–62.
- [16] Alan Lloyd Hodgkin. "The Ionic Basis of Electrical Activity in Nerve and Muscle". In: *Biological Reviews* 26.4 (1951), pp. 339–409.

- [17] Aaron G Blankenship and Marla B Feller. "Mechanisms Underlying Spontaneous Patterned Activity in Developing Neural Circuits". In: *Nature Reviews Neuroscience* 11.1 (2010), p. 18.
- [18] Carlo Alberto Maggi and Alberto Meli. "The Sensory-Efferent Function of Capsaicin-Sensitive Sensory Neurons". In: *General Pharmacology: The Vascular System* 19.1 (1988), pp. 1–43.
- [19] YEHEZKEL Ben-Ari et al. "Giant Synaptic Potentials in Immature Rat CA3 Hippocampal Neurones." In: *The Journal of Physiology* 416.1 (1989), pp. 303–325.
- [20] Philip A Schwartzkroin and David A Prince. "Cellular and Field Potential Properties of Epileptogenic Hippocampal Slices". In: *Brain Research* 147.1 (1978), pp. 117–130.
- [21] Naohide Yamashita, Naohiko Shibuya, and Etsuro Ogata. "Hyperpolarization of the Membrane Potential Caused by Somatostatin in Dissociated Human Pituitary Adenoma Cells that Secrete Growth Hormone". In: *Proceedings of the National Academy of Sciences* 83.16 (1986), pp. 6198–6202.
- [22] ILAN Lampl and YOSEF Yarom. "Subthreshold Oscillations of the Membrane Potential: A Functional Synchronizing and Timing Device". In: *Journal of neurophysiology* 70.5 (1993), pp. 2181–2186.
- [23] Rodolfo R Llinás. "The Intrinsic Electrophysiological Properties of Mammalian Neurons: Insights Into Central Nervous System Function". In: *Science* 242.4886 (1988), pp. 1654–1664.
- [24] Diego Contreras. "Electrophysiological Classes of Neocortical Neurons". In: *Neural Networks* 17.5-6 (2004), pp. 633–646.
- [25] John A Assad et al. "Brain Function: Novel Technologies Driving Novel Understanding". In: *Bioinspired Approaches for Human-Centric Technologies*. Springer, 2014, pp. 299–334.
- [26] Claire Wood, Christine Williams, and Gareth J Waldron. "Patch Clamping by Numbers". In: *Drug Discovery Today* 9.10 (2004), pp. 434–441.
- [27] Yasuhiko Jimbo et al. "A System for MEA-Based Multisite Stimulation". In: *IEEE Transactions on Biomedical Engineering* 50.2 (2003), pp. 241–248.
- [28] Shimon Marom and Goded Shahaf. "Development, Learning and Memory in Large Random Networks of Cortical Neurons: Lessons Beyond Anatomy". In: *Quarterly Reviews of Biophysics* 35.1 (2002), pp. 63–87.
- [29] Rolf Weis and Peter Fromherz. "Frequency Dependent Signal Transfer in Neuron Transistors". In: *Physical Review E* 55.1 (1997), p. 877.
- [30] Alan L Hodgkin and Andrew F Huxley. "A Quantitative Description of Membrane Current and its Application to Conduction and Excitation in Nerve". In: *The Journal of physiology* 117.4 (1952), pp. 500–544.
- [31] Douglas J Bakkum et al. "Tracking Axonal Action Potential Propagation on a High-Density Microelectrode Array Across Hundreds of Sites". In: *Nature Communications* 4 (2013), p. 2181.
- [32] Marie Engelen J Obien et al. "Revealing Neuronal Function through Microelectrode Array Recordings". In: *Frontiers in Neuroscience* 8 (2015), p. 423.
- [33] David A Robinson. "The Electrical Properties of Metal Microelectrodes". In: *Proceedings of the IEEE* 56.6 (1968), pp. 1065–1071.

- [34] Matthew J Nelson et al. "Review of Signal Distortion Through Metal Microelectrode Recording Circuits and Filters". In: *Journal of Neuroscience Methods* 169.1 (2008), pp. 141–157.
- [35] Andreas Hierlemann et al. "Growing Cells atop Microelectronic Chips: Interfacing Electrogenic Cells in vitro with CMOS-Based Microelectrode Arrays". In: *Proceedings of the IEEE* 99.2 (2010), pp. 252–284.
- [36] Michele Fiscella et al. "Recording from Defined Populations of Retinal Ganglion Cells using a High-Density CMOS-Integrated Microelectrode Array with Real-Time Switchable Electrode Selection". In: *Journal of Neuroscience Methods* 211.1 (2012), pp. 103–113.
- [37] Urs Frey et al. "Microelectronic System for High-Resolution Mapping of Extracellular Electric Fields Applied to Brain Slices". In: *Biosensors and Bioelectronics* 24.7 (2009), pp. 2191–2198.
- [38] Lucian Medrihan et al. "Asynchronous GABA Release is a Key Determinant of Tonic Inhibition and Controls Neuronal Excitability: A Study in the Synapsin II-/- Mouse". In: *Cerebral cortex* 25.10 (2014), pp. 3356–3368.
- [39] Roeland Huys et al. "Single-Cell Recording and Stimulation with a 16k Micro-Nail Electrode Array Integrated on a 0.18  $\mu\text{m}$  CMOS Chip". In: *Lab on a Chip* 12.7 (2012), pp. 1274–1280.
- [40] A Odawara et al. "Long-Term Electrophysiological Activity and Pharmacological Response of a Human Induced Pluripotent Stem Cell-Derived Neuron and Astrocyte Co-Culture". In: *Biochemical and biophysical research communications* 443.4 (2014), pp. 1176–1181.
- [41] Hayder Amin et al. "Electrical Responses and Spontaneous Activity of Human iPS-Derived Neuronal Networks Characterized for 3-Month Culture with 4096-Electrode Arrays". In: *Frontiers in Neuroscience* 10 (2016), p. 121.
- [42] Amy J Wagers and Irving L Weissman. "Plasticity of Adult Stem Cells". In: *Cell* 116.5 (2004), pp. 639–648.
- [43] In-kyung Park et al. "Bmi-1 is Required for Maintenance of Adult Self-Renewing Haematopoietic Stem Cells". In: *Nature* 423.6937 (2003), p. 302.
- [44] Martin Körbling and Zeev Estrov. "Adult Stem Cells for Tissue Repair—A New Therapeutic Concept?" In: *New England Journal of Medicine* 349.6 (2003), pp. 570–582.
- [45] Jon S Odorico, Dan S Kaufman, and James A Thomson. "Multilineage Differentiation from Human Embryonic Stem Cell Lines". In: *Stem Cells* 19.3 (2001), pp. 193–204.
- [46] Kazutoshi Takahashi and Shinya Yamanaka. "Induction of Pluripotent Stem Cells from Mouse Embryonic and Adult Fibroblast Cultures by Defined Factors". In: *Cell* 126.4 (2006), pp. 663–676.
- [47] Kazutoshi Takahashi et al. "Induction of Pluripotent Stem Cells from Adult Human Fibroblasts by Defined Factors". In: *Cell* 131.5 (2007), pp. 861–872.
- [48] Junying Yu et al. "Induced Pluripotent Stem Cell Lines Derived from Human Somatic Cells". In: *Science* 318.5858 (2007), pp. 1917–1920.
- [49] Dirk Hockemeyer et al. "Efficient Targeting of Expressed and Silent Genes in Human ESCs and iPSCs using Zinc-Finger Nucleases". In: *Nature Biotechnology* 27.9 (2009), p. 851.

- [50] Michelle Christian et al. "Targeting DNA Double-Strand Breaks with TAL Effector Nucleases". In: *Genetics* 186.2 (2010), pp. 757–761.
- [51] Le Cong et al. "Multiplex Genome Engineering using CRISPR/Cas Systems". In: *Science* 339.6121 (2013), pp. 819–823.
- [52] Dirk Hockemeyer and Rudolf Jaenisch. "Induced Pluripotent Stem Cells Meet Genome Editing". In: *Cell Stem Cell* 18.5 (2016), pp. 573–586.
- [53] William Dauer and Serge Przedborski. "Parkinson's Disease: Mechanisms and Models". In: *Neuron* 39.6 (2003), pp. 889–909.
- [54] Joseph Jankovic. "Parkinson's Disease: Clinical Features and Diagnosis". In: *Journal of Neurology, Neurosurgery & Psychiatry* 79.4 (2008), pp. 368–376.
- [55] Sigurlaug Sveinbjornsdottir. "The Clinical Symptoms of Parkinson's Disease". In: *Journal of neurochemistry* 139 (2016), pp. 318–324.
- [56] A E Lang MD L V Kalia MD. "Parkinson's Disease". In: *The Lancet* 386 (2015), pp. 896–912.
- [57] Mihael H Polymeropoulos et al. "Mutation in the  $\alpha$ -synuclein gene identified in families with Parkinson's disease". In: *Science* 276.5321 (1997), pp. 2045–2047.
- [58] AB Singleton et al. " $\alpha$ -Synuclein Locus Triplication Causes Parkinson's Disease". In: *Science* 302.5646 (2003), pp. 841–841.
- [59] Jan Müller et al. "High-Resolution CMOS MEA Platform to Study Neurons at Subcellular, Cellular, and Network Levels". In: *Lab on a Chip* 15.13 (2015), pp. 2767–2780.
- [60] Tiziano Barberi et al. "Neural Subtype Specification of Fertilization and Nuclear Transfer Embryonic Stem Cells and Application in Parkinsonian Mice". In: *Nature Biotechnology* 21.10 (2003), p. 1200.
- [61] FUJIFILM Cellular Dynamics. *iCell DopaNeurons*. <https://fujifilmcdi.com/products-services/icell-products/icell-dopaneurons/>. July 13, 2019.
- [62] FUJIFILM Cellular Dynamics. *MyCell DopaNeurons(A53T)*. <https://fujifilmcdi.com/products-services/icell-products/mycell-dopaneurons-a53t/>. July 13, 2019.
- [63] Benoit I Giasson et al. "Neuronal  $\alpha$ -Synucleinopathy with Severe Movement Disorder in Mice Expressing A53T Human  $\alpha$ -Synuclein". In: *Neuron* 34.4 (2002), pp. 521–533.
- [64] FUJIFILM Cellular Dynamics. *iCell Astrocytes*. <https://fujifilmcdi.com/products-services/icell-products/icell-astrocytes/>. July 13, 2019.
- [65] Suzanne Lesage et al. "Large-Scale Screening of the Gaucher's Disease-Related Glucocerebrosidase Gene in Europeans with Parkinson's Disease". In: *Human Molecular Genetics* 20.1 (2010), pp. 202–210.
- [66] Sonja Kriks et al. "Dopamine Neurons Derived from Human ES Cells Efficiently Engraft in Animal Models of Parkinson's Disease". In: *Nature* 480.7378 (2011), p. 547.
- [67] Stefania Fedele et al. "Expansion of Human Midbrain Floor Plate Progenitors from Induced Pluripotent Stem Cells Increases Dopaminergic Neuron Differentiation Potential". In: *Scientific Reports* 7.1 (2017), p. 6036.
- [68] MaxWell Biosystems. *MaxOne MEA Wells*. <https://www.mxwbio.com/products/maxone-mea-system-microelectrode-array/maxone-mea-wells/>. July 3, 2019.

- [69] Marco Ballini et al. “A 1024-Channel CMOS Microelectrode Array with 26,400 Electrodes for Recording and Stimulation of Electrogenic Cells In Vitro”. In: *IEEE Journal of Solid-State Circuits* 49.11 (2014), pp. 2705–2719.
- [70] Pierre Yger et al. “A Spike Sorting Toolbox for up to Thousands of Electrodes Validated with Ground Truth Recordings in Vitro and in Vivo”. In: *ELife* 7 (2018), e34518.
- [71] Cyrille Rossant et al. “Spike Sorting for Large, Dense Electrode Arrays”. In: *Nature Neuroscience* 19.4 (2016), p. 634.
- [72] Gaute T Einevoll et al. “Towards Reliable Spike-Train Recordings from Thousands of Neurons with Multielectrodes”. In: *Current Opinion in Neurobiology* 22.1 (2012), pp. 11–17.
- [73] JM Deniau et al. “Electrophysiological Properties of Identified Output Neurons of the Rat Substantia Nigra (Pars Compacta and Pars Reticulata): Evidences for the Existence of Branched Neurons”. In: *Experimental Brain Research* 32.3 (1978), pp. 409–422.
- [74] PG Guyenet and GK Aghajanian. “Antidromic Identification of Dopaminergic and Other Output Neurons of the Rat Substantia Nigra”. In: *Brain Research* 150.1 (1978), pp. 69–84.
- [75] James M Tepper et al. “Autoreceptor-Mediated Changes in Dopaminergic Terminal Excitability: Effects of Striatal Drug Infusions”. In: *Brain Research* 309.2 (1984), pp. 309–316.
- [76] Seung U Kim, Kenneth G Warren, and Madhu Kalia. “Tissue Culture of Adult Human Neurons”. In: *Neuroscience Letters* 11.2 (1979), pp. 137–141.
- [77] Cedric Bardy et al. “Neuronal Medium that Supports Basic Synaptic Functions and Activity of Human Neurons in Vitro”. In: *Proceedings of the National Academy of Sciences* 112.20 (2015), E2725–E2734.



# Gustavo Prack

## Curriculum Vitae

*"Master's student of Nanoscience at the University of Basel in Switzerland, with focus on neurobiology and condensed matter physics."*

### Education

- 02/2017- **Master of Science in Nanosciences (Physics)**, *University of Basel*, Basel.  
Present **Study emphases:** Neurobiology and Condensed Matter Physics  
First project work at the *University of Basel*:  
- "KPFM Measurements of High Efficiency CIGS- and Perovskite Solar Cells"  
Second project work at the *ETH Zürich*:  
- "Development of a Novel Electrophysiological Measurement Tool *In Vitro* using AC-SECM"  
Master's thesis at the Bio Engineering Laboratory, *ETH Zürich*:  
- "Studying the Electrophysiological Phenotype of Human Dopaminergic Neurons with High-Density Microelectrode Arrays"
- 09/2013- **Bachelor of Science in Nanosciences**, *University of Basel*, Basel.  
01/2017 8 Block courses (equivalent to Bachelor's thesis):  
- "Graphene Growth on Ni(100) by UHV Chemical Vapour Deposition"  
- "Fabrication of Hall Bar Structures on Gallium Arsenide Wafer Surfaces"  
- "Programming of a Pipetting Robot to Study Parkinson's Disease"  
- "Magnetic Refrigeration on a Pulse Tube Platform"  
- "Microscopy"  
- "Polymer Vesicles as a Mode of Transportation through Nuclear Pore Complexes"  
- "Reaction Between Sympathetically Cooled  $O_2^+$  Ions with a Beam of COS"  
- "Muon Spin Rotation/Relaxation Spectroscopy of  $Mo_8Ga_{41}$  and  $EuTiO_3$ "
- 08/2007- **Swiss High School Degree ("Matura")**, *Gymnasium Bäumlhof*, Basel.  
06/2012 **Study emphases:** Biology and Chemistry

### Professional Experience

- 02/2016- **Math Teaching Assistant**, *University of Basel*, Basel.  
05/2017 - Tutor in Mathematics I for students of natural sciences  
- Tutor in Mathematics II for students of natural sciences

Steingrubenweg 63 – Riehen 4125, Basel-Stadt, Switzerland

☎ +41 76 422 63 74 • ✉ [gustavo.prack@unibas.ch](mailto:gustavo.prack@unibas.ch)

Date of birth: 26<sup>th</sup> of July, 1993

---

## Languages

German **Native language**  
Portuguese **Native language**  
(Brazilian)  
English **Fluent**  
French **Intermediate**

---

## Awards

2011 **1<sup>st</sup> Place**, *Science On the Move*.  
The nation-wide Swiss class competition in biology and biochemistry